JGR Biogeosciences

RESEARCH ARTICLE
10.1029/2020JG006124

Key Points:

- High CO_2, CH_4, and N_2O concentrations in urbanized river reaches reflect influences from local tributaries carrying wastewater
- Seasonality in stable C isotopes and dissolved organic matter properties corresponds to higher dry-season greenhouse gas concentrations than in the monsoon
- Stable C isotopes and their relationships with CO_2 and CH_4 concentrations support localized wastewater effects on urbanized rivers

Supporting Information:

Supporting Information may be found in the online version of this article.

Correspondence to:

J.-H. Park,
jhp@ewha.ac.kr

Citation:

Begum, M. S., Bogard, M. J., Butman, D. E., Chea, E., Kumar, S., Lu, X., et al. (2021). Localized pollution impacts on greenhouse gas dynamics in three anthropogenically modified Asian river systems. *Journal of Geophysical Research: Biogeosciences*, *126*, e2020JG006124. https://doi.org/10.1029/2020JG006124

Received 19 OCT 2020
Accepted 28 APR 2021

Localized Pollution Impacts on Greenhouse Gas Dynamics in Three Anthropogenically Modified Asian River Systems

Most Shirina Begum[1], Matthew J. Bogard[2,3], David E. Butman[3,4], Eliyan Chea[5], Sanjeev Kumar[6], Xixi Lu[7], Omme K. Nayna[1], Lishan Ran[8], Jeffrey E. Richey[9], Shafi M. Tareq[10], Do Thi Xuan[11], Ruihong Yu[12], and Ji-Hyung Park[1]

[1]Department of Environmental Science and Engineering, Ewha Womans University, Seoul, Republic of Korea, [2]Now at Department of Biological Sciences, University of Lethbridge, Lethbridge, AB, Canada, [3]School of Environmental and Forest Sciences, University of Washington, Seattle, WA, USA, [4]Department of Civil and Environmental Engineering, University of Washington, Seattle, WA, USA, [5]Department of Environmental Science, Royal University of Phnom Penh, Phnom Penh, Cambodia, [6]Geosciences Division, Physical Research Laboratory, Ahmedabad, India, [7]Department of Geography, National University of Singapore, Singapore, [8]Department of Geography, The University of Hong Kong, Hong Kong, China, [9]School of Oceanography, University of Washington, Seattle, WA, USA, [10]Department of Environmental Sciences, Jahangirnagar University, Dhaka, Bangladesh, [11]Biotechnology Research and Development Institute, Can Tho University, Cantho, Vietnam, [12]Inner Mongolia Key Lab of River and Lake Ecology, University of Inner Mongolia, Hohhot, China

Abstract

Despite growing research on greenhouse gas (GHG) emissions from inland waters, few systematic efforts have been made to assess the regional-scale GHG emissions from Asian rivers under increasing anthropogenic stress. We examined factors controlling longitudinal and seasonal variations in the partial pressure of CO_2 (pCO_2), and CH_4 and N_2O concentrations in the Ganges, Mekong, and Yellow River by simultaneously measuring gas concentrations and stable C isotopes, and optical properties of dissolved organic matter (DOM) from 2016 to 2019. The levels of pCO_2 and CH_4 were distinctively higher in polluted tributaries and affected reaches of the Ganges and Mekong than in the Yellow River. The highest levels of N_2O were found in the Ganges, followed by the Yellow River and Mekong. Across these basins, dry-season mean concentrations of CO_2, CH_4, and N_2O were 1.6, 2, and 7 times higher than those measured in the monsoon season, respectively. This seasonality was consistent with that of $\delta^{13}C$-CO_2, while $\delta^{13}C$-CH_4 showed an opposite pattern. GHG concentrations exhibited significant positive relationships with DOM concentrations and optical properties including fluorescence index and protein-like fluorescence, implying the contribution of anthropogenic, labile DOM to production of GHGs in the polluted reaches. Graphical mixing models of $\delta^{13}C$-CO_2 and $\delta^{13}C$-CH_4 support the stronger impact of wastewater on the Ganges and Mekong than on the Yellow River. The overall results suggest that neglecting localized pollution impacts on GHG emissions from increasingly urbanized river basins can result in a substantial underestimation of global riverine GHG emissions.

Plain Language Summary

Rapid urbanization and poor wastewater infrastructure are turning many large rivers in Asia into significant sources of greenhouse gases (GHGs). We examined controlling factors for the concentrations of CO_2, CH_4, and N_2O in the Ganges, Mekong, and Yellow River by simultaneously measuring gas concentrations and stable carbon isotopes, and optical properties of dissolved organic matter (DOM). The concentrations of CO_2 and CH_4 were distinctively higher in polluted tributaries and affected sections of the Ganges and Mekong than in the Yellow River. N_2O concentration was highest in the Ganges, followed by the Yellow River and Mekong. Across these basins, the concentrations of the three gases were generally higher during dry periods than in the monsoon season. GHG concentrations were positively related to DOM optical properties indicating the contribution of easily degradable DOM from pollution sources. The stable carbon isotope ratios of CO_2 and CH_4 support the stronger impact of wastewater on the Ganges and Mekong than on the Yellow River. The overall results suggest that neglecting local pollution impacts on GHG emissions from increasingly urbanized river basins can result in a substantial underestimation of global riverine GHG emissions.

1. Introduction

Inland waters including rivers, streams, lakes, and reservoirs have increasingly been recognized as "active pipes" transforming and exchanging organic matter (OM) with floodplains, sediments, and the atmosphere during transport to the oceans (Aufdenkampe et al., 2011; Cole et al., 2007). Inland waters are also significant sources of greenhouse gases (GHGs) (Bastviken et al., 2011; Borges et al., 2015; Richey et al., 1988). The global inland water emissions of CO_2, CH_4, and N_2O are estimated at 7.7 (Raymond et al., 2013), 0.75 (Stanley et al., 2016), and 0.52 Pg CO_2-equivalent (CO_2eq) yr^{-1} (Kroeze et al., 2010), respectively, which are of similar magnitude as the oceanic (9.2 Pg CO_2eq yr^{-1}) and terrestrial (11.7 Pg CO_2eq yr^{-1}) sinks of anthropogenic CO_2 (Friedlingstein et al., 2019). GHG emissions associated with active transformations of OM in inland waters are vulnerable to anthropogenic activities such as water pollution and impoundments (Marescaux et al., 2018; Regnier et al., 2013). For instance, polluted rivers in Europe have been reported as significant sources of CO_2 and other GHGs with substantial proportions of gas emissions attributable to labile OM released from anthropogenic sources (Borges, Darchambeau, et al., 2018; Frankignoulle et al., 1998). However, the effect of altered riverine metabolic processes on GHG emissions from anthropogenically modified rivers is poorly understood, particularly in the developing countries that are underrepresented in global riverine GHG budgets. Furthermore, field measurements of riverine GHGs have focused on CO_2 (Abril et al., 2014; Butman & Raymond, 2011; Ran et al., 2017), while concurrent measurements of the multiple GHGs have been related to a single anthropogenic stress, such as agriculture (Borges, Darchambeau, et al., 2018), urbanization (Li et al., 2020; Wang et al., 2017), and river impoundment (Deemer et al., 2016).

The traditional concept of the river continuum (Vannote et al., 1980) has been criticized for its inability to account for discontinuities in riverine biogeochemical processes along the reaches affected by dams, wastewater, and other perturbations (Park et al., 2018). The emissions of GHGs from impounded waters vary with time; for instance, high emissions of GHGs within years of dam construction have been associated with the degradation of flooded terrestrial OM (Deemer et al., 2016; Teodoru et al., 2012). Eutrophic reservoirs facilitate primary production in the epilimnion, reducing CO_2 emissions (Ran et al., 2017). Consequently, phytoplankton-derived OM and nutrients accumulated in benthic sediments create anoxic conditions that can either facilitate CH_4 and N_2O production (Deemer et al., 2016) or N_2O consumption. Concomitantly, large amounts of wastewater ($>500 \times 10^6$ m^3) return to rivers carrying nutrients and particulate and dissolved OM (POM and DOM, respectively) (Park et al., 2018; Ulliman et al., 2020). Discharge from wastewater treatment plants (WWTPs) can significantly contribute to GHG emissions from downstream rivers (Begum et al., 2019; Garnier et al., 2013; Jin et al., 2018; Wang et al., 2017; Yoon et al., 2017). A laboratory incubation experiment showed that untreated wastewater can generate significantly higher amounts of CO_2 than treated wastewater (Kim et al., 2019).

While accounting for only 29% of global river-surface area, Asian rivers contribute ~35% of global freshwater discharge and 50% and 39% of total organic C (TOC) and dissolved inorganic C (DIC) exports to the oceans, respectively (Degens et al., 1991; Hu et al., 2016). Consequently, Asian rivers are significant contributors to global riverine GHG emissions; for instance, N_2O emissions from Asian rivers account for 33% (32.2 Gg N_2O-N yr^{-1}) of the global riverine emission (Hu et al., 2016). Despite large uncertainties in estimating CO_2 and CH_4 emissions from Asian rivers due to scarcity of field measurements (Park et al., 2018), CO_2 emissions from SE Asian rivers were estimated to exceed 10 g C m^{-2} yr^{-1}, similar to rates observed in large tropical rivers, that is, the Amazon and Congo (Lauerwald et al., 2015). Large dams in Asia (1,906 dams with surface areas >0.1 km^2) were estimated to have a total storage capacity 1,625 km^3 (Lehner et al., 2011), representing an important anthropogenic perturbation to riverine biogeochemical fluxes. Rivers across Asia are highly polluted with domestic and industrial wastewater and agricultural runoff that may amount to 144×10^9 m^3 yr^{-1} (Evans et al., 2012). Accordingly, GHG emissions from Asian rivers are expected to be comparatively high, demanding more field measurements of GHG concentrations and associated environmental factors to better constrain these fluxes on a continental scale.

To examine longitudinal and seasonal variations in the three major GHGs (CO_2, CH_4, and N_2O) in Asian rivers, the Ganges, Mekong, and Yellow River (Huang He) were selected for an exploratory field study based on their length, basin size, annual discharge, and anthropogenic disturbances. They represent large Asian rivers under increasing anthropogenic stresses such as hydroelectric dams, reservoirs for irrigation, wastewater from increasing urbanization, and agricultural runoff (He et al., 2017; Whitehead et al., 2015).

The primary objective was to assess human impacts on the riverine dynamics of the three GHGs and DOM in these basins. Specifically, we explored the spatial and seasonal variations in surface water concentrations of the three GHGs and their associations with anthropogenic alterations of the river continuum caused by wastewater and dams. We hypothesized that (a) localized effects of pollution can create longitudinal discontinuities in riverine fluxes of GHGs and OM, (b) production of GHGs is enhanced during the dry season when a greater proportion of river flow is derived from wastewater, and (c) stable C isotopes in CO_2 and CH_4 can reveal predominant sources of GHGs. In order to elucidate the mechanisms controlling riverine dynamics of the three GHGs across the anthropogenically modified reaches of the three rivers, we focused on GHG concentrations, complemented with ancillary water quality data. By combining simultaneous measurements of three GHGs and DOM properties in three understudied large Asian rivers, the basin-scale field measurements were expected to provide baseline data for assessing anthropogenic perturbations to riverine organic C fluxes and GHG emissions as a consequence of increasing river pollution and impoundments across Asia.

2. Materials and Methods

2.1. Study Sites

The Ganges, Mekong, and Yellow River, which originate in the Himalayan mountains and/or Tibetan Plateau, drain some of the largest watersheds in the world with a total area exceeding $2{,}500 \times 10^3$ km^2 (Milliman & Farnsworth, 2011). These river systems share common hydrologic and demographic features, including intense monsoon-driven seasonality in discharge and high population densities in the river basin (Park et al., 2018). More detailed information on each of these river basins is provided in Supporting Information. Monsoon rains support a population of 400 million (8% of the global population) in the Ganges (Park et al., 2018; Parua, 2010), 70 million in the Mekong (MRC, 2019), and 107 million (~9% of China's total population) in the Yellow River basins (Gao & Wang, 2017). These large populations use river water for irrigation, and industrial and domestic consumption; consequently, numerous dams and reservoirs have been constructed on many rivers over the last few decades (Lehner et al., 2011). For instance, there are 81–142, 241, and 3,150 large dams on the Ganges (Dutta et al., 2020; Lehner et al., 2011), Mekong (WLE-Mekong, 2020), and Yellow River basins (Wang et al., 2006), respectively. The three rivers receive large loads of poorly treated or untreated wastewater from the increasingly urbanized watersheds (Mekonnen & Hoekstra, 2018; Park et al., 2018; Sato et al., 2013). The Ganges receives annually about $1{,}186 \times 10^6$ tons of sewage from the metropolitan areas, and only 757×10^6 tons are treated before discharging into the river (CPCB, 2013; Dutta et al., 2020). The Yellow River receives 45×10^6 tons of wastewater every year, with 90% being treated (Qi et al., 2020; Zhao et al., 2020). Basin-specific wastewater information is not available for the Mekong, but the pollution loads have been found to exceed the natural assimilation capacity of the basin (Mekonnen & Hoekstra, 2018).

Field investigations were conducted in multiple mainstem sections of the three rivers and local tributaries or wastewater drains between August 2016 and July 2019 (Figure 1). The major tributaries of the Ganges include the Gomti, Ghaghara, Gandak, Kosi, Yamuna, Son, Punpun, and Damodar in India, while the Brahmaputra and Meghna rivers flow into the mainstem river in Bangladesh (Parua, 2010). The Yamuna, the longest tributary flowing parallel to the upper mainstem called Ganga, was considered the mainstem in this study. Therefore, the main branches of the Ganges (termed "mainstem") include two parallel branches traversing northern India, that is, the Ganga and Yamuna, as well as two bifurcated distributaries, that is, the Hooghly in India, and the Padma flowing from the Farakka Barrage across Bangladesh to the Bay of Bengal. The mainstem of the Mekong River consists of the Lancang (the upper Mekong) flowing through the Yunnan province of China and the lower Mekong River flowing through Myanmar, Laos, Thailand, Cambodia, and Vietnam. A single mainstem constitutes the Yellow River, which flows from the Tibetan Plateau through the Loess Plateau to the Northern China Plain.

The mainstems of the three rivers were divided into three reaches: "upper," "middle," and "lower" (Table S1). As local sources of pollution, urban tributaries and wastewater drains (termed "T&W") were sampled together with the polluted mainstem reaches within or downstream of the major metropolitan areas of the Ganges (Delhi, Kanpur, Varanasi, Kolkata, and Dhaka), the lower Mekong (Chiang Rai, Phnom Penh, and Cantho), and the middle reach of the Yellow River (Hohhot and the agricultural areas in Loess Plateau)

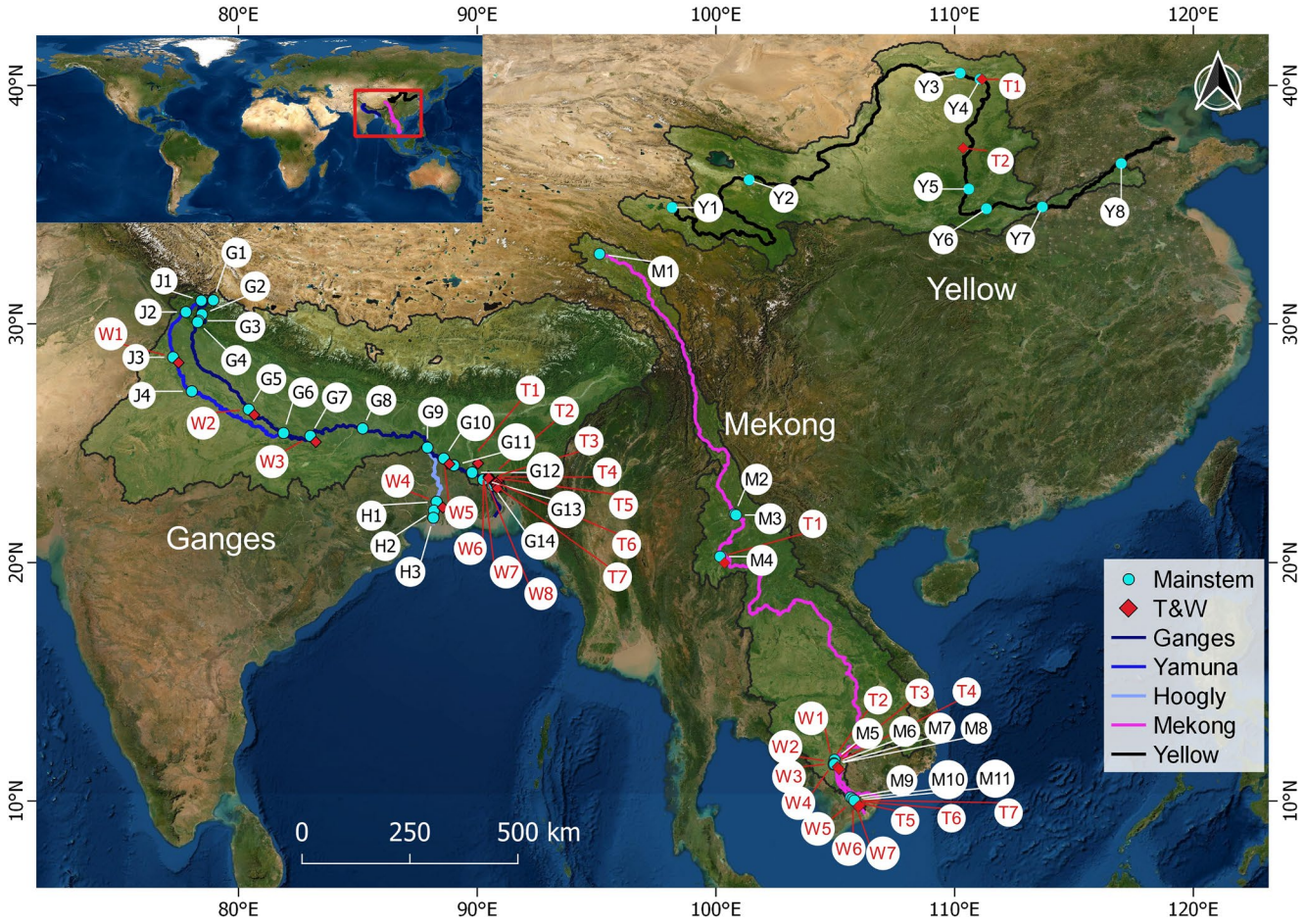

Figure 1. Sampling locations in three large Asian river basins—the Ganges (n = 36), Mekong (n = 25), and Yellow River (n = 10). Samples collected from the mainstem sites (n = 40) are indicated by circles, while tributaries (T; n = 16) and wastewater drains (W; n = 15) are indicated by diamonds.

(Figure 1). Water and gas samples were collected from 71 locations, including 36 in the Ganges, 25 in the Mekong, and 10 in the Yellow River during the monsoon season. Sampling was repeated at 35 sites during the dry season for seasonal comparison (Figure 1; Table S1). To complement the minimal tributary data in the Yellow River basin, the published data of the partial pressure of CO_2 (pCO_2) in the Wuding River draining Loess Plateau (Ran et al., 2017) was included as part of the middle reach.

2.2. Sample Collection and In Situ Measurements

Water samples were collected at a depth of 10–20 cm below the water surface, using a polycarbonate bottle or portable water sampler (Masterflex E/S, Cole-Parmer, USA). Samples were immediately frozen and within a week shipped in an icebox to Korea for laboratory analysis. At each sampling point, in situ water quality parameters, including water temperature, pH, dissolved oxygen (DO), and electrical conductivity, were measured using a portable multiparameter meter (Orion 5-Star Portable, Thermo Scientific, USA). Dissolved gas samples were collected at the same water depth (10–20 cm below the water surface) using a manual headspace equilibration method (Yoon et al., 2016). Headspace equilibration was performed for 2 min using a 60 mL polypropylene syringe filled with a 30 mL water sample and a 30 mL ambient air sample. Approximately 20 mL of the equilibrated air was transferred to a pre-evacuated 12 mL Exetainer vial. Air temperature and barometric pressure were measured in situ using a portable sensor (Watchdog 1650 Micro Station, Spectrum Technologies, USA). When direct measurements were not possible for some

samplings in the Ganges ($n = 17$), Mekong ($n = 20$), and Yellow River ($n = 5$), meteorological data were collected from the nearest location using an internet source (timeanddate.com).

2.3. GHGs and Stable C Isotope Measurements

The equilibrated headspace air samples and the ambient air samples were analyzed using a gas chromatograph (7890A, Agilent, USA) that was equipped with a flame ionization detector coupled with a methanizer (for CH_4 and CO_2 analysis) and a microelectron capture detector (for N_2O analysis), as described in detail by Jin et al. (2018). The gas chromatography signals were calibrated prior to sample analysis using standard reference gases, that is, three GHGs in a balance of N_2 (RIGAS Corporation, Korea). The barometric pressure and water temperature were used to calculate concentrations of the three GHGs from the gas concentrations in the equilibrated air and ambient air samples, based on Henry's law (Hudson, 2004). The stable C isotope ratios of CO_2 and CH_4 in another set of headspace-equilibrated samples were analyzed using an isotopic analyzer (G2201-*i*, Picarro, USA) in a laboratory at the University of Washington. Equilibrated gas samples were injected into the analyzer using the small sample introduction module 2 (SSIM2). Standards of CO_2 (−31.5‰) and CH_4 (−38.3 ‰) were injected prior to sample processing as well as at the end of some runs, to confirm that instrument drift did not occur. Isotopic ratios of equilibrated headspace gases were then used to determine values for gas in the water, as described by Hamilton and Ostrom (2007). Isotopic fractionation between dissolved and gaseous phases at equilibrium was calculated for $\delta^{13}C\text{-}CO_2$, according to the temperature-based equation from Mook et al. (1974), and for $\delta^{13}C\text{-}CH_4$, according to the approach followed by Knox et al. (1992). Gas concentrations in dissolved phase at equilibrium were calculated using Henry's constant, corrected for temperature at time of sampling (Weiss, 1974), and solubility of CH_4 (Gevantman, 2010). The stable isotopic composition of C is reported using delta notation, where $\delta^{13}C = (R_{sample}/R_{standard}) - 1$. Here, R_{sample} and $R_{standard}$ are ratios of heavy to light isotopes (^{13}C:^{12}C) in the sample (R_{sample}) and standard ($R_{standard}$) of Vienna Pee Dee Belemnite.

2.4. Water Analysis

Thawed water samples were filtered through pre-combusted glass fiber filters (GF/F; Whatman, nominal pore size 0.7 μm) to remove suspended materials. The total suspended solid (TSS) was measured gravimetrically as the difference in the filter weight before and after filtering and drying at 60 °C for 48 h. The concentrations of particulate organic C and N (POC and PON) in the TSS were measured using an elemental analyzer (Flash 2000, Thermo Fisher Scientific, Germany). The subsamples for POC measurement were acidified/fumigated with HCl before analysis to remove inorganic C fraction, whereas PON measurements were performed in untreated samples. The concentration of dissolved organic carbon (DOC) in a filtered sample was measured using a total organic carbon analyzer based on high-temperature combustion of OM followed by thermal detection of CO_2 (TOC-V_{CPH}, Shimadzu, Japan). Filtered samples were also analyzed for major inorganic ions including NO_3^-, NH_4^+, and PO_4^- (883 Basic IC Plus, Metrohm, Switzerland). Dissolved inorganic N (DIN) was determined as the sum of the N concentrations in NO_3^- and NH_4^+. For quality control, standards with known concentrations and ultrapure water were analyzed after every ten-sample batch, and triplicate analysis was performed for approximately 10% of all the samples to assess instrumental stability and accuracy.

Ultraviolet (UV) absorbance was measured across a wavelength range of 200–1,100 nm using a UV-Vis spectrophotometer, and the measurements were used to determine the specific UV absorbance at 254 nm ($SUVA_{254}$) (Helms et al., 2008; Weishaar et al., 2003). Fluorescence excitation-emission matrices (EEMs) were collected on a fluorescence spectrophotometer (F7000, Hitachi, Japan) by simultaneously scanning excitation wavelengths from 200 to 400 nm, at 5 nm intervals, and emission wavelengths from 290 to 540 nm, at 1 nm intervals (Begum et al., 2019). Fluorescence-based indices were obtained from the corrected EEMs, including the humification index (HIX; Zsolnay et al., 1999), fluorescence index (FI; McKnight et al., 2001), and biological index (Huguet et al., 2009). To identify the major components of the obtained EEMs, parallel factor (PARAFAC) analysis was conducted using the DOM Fluor toolbox (http://www.models.life.ku.dk) on MATLAB 7.1 (Mathworks, USA) based on a method developed by Stedmon and Bro (2008). Fluorescent DOM (FDOM) components were validated by visual inspection of the residuals and split-half analysis (Stedmon & Bro, 2008).

2.5. Statistical Analysis

All statistical analyses were conducted after applying the Shapiro-Wilk test to examine the normal distribution of the data using SigmaPlot (Systat, USA) or R (R Development Core Team, 2020). Linear regressions were conducted to explore significant relationships between the concentrations of the three GHGs in the Ganges, Mekong, and Yellow River. To analyze significant differences in GHG concentrations and their stable C isotopes among the mainstem reaches and T&W, a one-way analysis of variance (ANOVA) followed by Tukey's HSD or a one-way ANOVA on ranks using the Kruskal-Wallis method, followed by Dunn's test were conducted depending on the distribution of the data. Seasonal variations in the concentrations and stable C isotopes of GHGs were analyzed using the Wilcoxon signed-rank test due to nonnormal distribution of data. The relationships between the three GHGs and water quality parameters were analyzed by best-fit regressions on SigmaPlot. Principal component analysis (PCA) was conducted with the data of GHGs, OM, and other water quality parameters using R. The significance level was set at $P < 0.05$, unless indicated otherwise.

To identify and distinguish different sources of CO_2 and CH_4, we used two graphical mixing models, that is, Keeling plot and Miller-Tans plot. Based on the principle of conservation of mass and mixing of isotopically distinct C sources, both models have been successfully applied to identify the primary sources of riverine DIC and GHGs (Campeau et al., 2017; O'Dwyer et al., 2020). In the Keeling plot approach, an isotopic source is obtained from the *y*-intercept of a plot consisting of $\delta^{13}C$ values and 1/C concentrations (Keeling, 1958). The Keeling plot is usually used for simple systems with a known background $\delta^{13}C$ and a single source, and thus cannot function properly in cross-system studies with multiple sources and sinks (O'Dwyer et al., 2020). The Miller-Tans plot approach accounts for inconsistency in the background $\delta^{13}C$ and works better in cross-system studies (Campeau et al., 2017; O'Dwyer et al., 2020). In the Miller-Tans plot approach, an isotopic source is obtained from the slope of the regression between $\delta^{13}C$ and the product of $\delta^{13}C$ and C concentrations (Miller & Tans, 2003). We used the Miller-Tans plot approach in this interbasin study to identify and interpret potential difference in $\delta^{13}C$ sources in the Ganges, Mekong, and Yellow River.

3. Results

3.1. Spatiotemporal Variations in CO_2, CH_4, and N_2O

3.1.1. Overview of Interbasin and Seasonal Variations in GHG Concentrations

Across the three river basins, CO_2, CH_4, and N_2O were supersaturated at most sites with respect to the levels at atmospheric equilibrium, which corresponded to 437 μatm, 0.005 μM, and 5.4 nM, respectively (Table 1; Begum et al., 2021). The mean concentrations of all three gases in the mainstem were highest in the Ganges, reflecting exceptionally high gas concentrations found in the highly polluted tributaries and middle reach. While the middle and lower reaches of the Mekong and Yellow River exhibited similar levels of the three gases, pCO_2 and CH_4 concentrations at T&W sites tended to be higher in the Mekong, contrasting with the higher concentrations of N_2O in the Yellow River. Regression analysis showed a significant positive relationship between CO_2 and CH_4 concentrations for both the Ganges and the Mekong (Figure 2). N_2O concentrations in the Yellow River were positively related to both CO_2 and CH_4 concentrations, with much steeper slopes than the corresponding regressions for the Ganges (Figure 2). Across the three basins, the concentrations of CO_2 and CH_4 exhibited significant seasonal variation, with higher values during the dry season (Figures 3a and 3b). N_2O concentrations also tended to be higher during the dry season than during the monsoon season, but the seasonal difference was not significant at $P < 0.05$ (Figure 3c). $\delta^{13}C\text{-}CO_2$ was also significantly higher during the dry season, whereas a reversed seasonal pattern was found for $\delta^{13}C\text{-}CH_4$ (Figures 3d and 3e).

3.1.2. The Ganges River

The upper reaches of the Ganges, with low population density and few dams (Table S2), showed very low levels of pCO_2 and CH_4, averaging 340 μatm and 0.02 μM, respectively (Figure 4; Table 1). In the middle reaches traversing large metropolitan areas such as Delhi and Kanpur, pCO_2, CH_4, and N_2O averaged 5,695 μatm, 29.5 μM, and 42.7 nM, respectively (Figure 4; Table 1). T&W feeding into the middle

Table 1
Mean Concentrations and Ranges (Minimum–Maximum) of pCO_2, and CH_4 and N_2O Concentrations in the Upper, Middle, and Lower Reaches, and Tributaries and Wastewater Drains (T&W) of the Ganges, Mekong, and Yellow River Basins

		pCO_2 (μatm)			CH_4 (μM)			N_2O (nM)		
River	Reach	*n*	Mean	Range	*n*	Mean	Range	*n*	Mean	Range
Ganges	Mainstem	30	2,385	(180–20,580)	31	8.9	(0.002–172.1)	31	18.4	(1.7–245.1)
	Upper	7	340^{ab}	(180–521)	8	0.02^{a}	(0.002–0.04)	8	9.0^{ab}	(7.6–11.0)
	Middle	9	5,695^{bc}	(825–20,580)	9	29.5^{b}	(0.34–172.1)	9	42.7^{ab}	(5.8–245.1)
	Lower	14	1,279^{b}	(285–3,165)	14	0.7^{ab}	(0.03–3.4)	14	8.1^{a}	(1.7–18.1)
	T&W	22	8,051^{c}	(664–27,290)	22	47.2^{b}	(0.06–234.8)	22	125.0^{b}	(0.5–1699.9)
Mekong	Mainstem	20	2,300	(433–3,729)	20	0.2	(0.01–2.2)	15	9.8	(2.2–17.9)
	Upper	1	1,552		1	0.01			ND	
	Middle	5	2,379^{ab}	(1,384–2,948)	5	0.1^{a}	(0.03–0.3)	5	10.6^{a}	(2.2–15.3)
	Lower	14	2,325^{a}	(433–3,729)	14	0.3^{a}	(0.01–2.2)	10	9.4^{a}	(2.9–17.9)
	T&W	25	7,536^{b}	(1,101–34,151)	24	45.5^{b}	(0.3–455.8)	17	30.5^{a}	(3.5–197.9)
Yellow	Mainstem	9	1,921	(694–4,861)	9	0.4	(0.06–2.0)	7	13.9	(3.7–35.8)
	Upper	2	976	(694–1,258)	2	1.0	(0.08–2.0)		ND	
	Middle	5	2,475	(1,253–4,861)	5	0.2	(0.06–0.3)	5	14.7	(3.7–35.8)
	Lower	2	1,478	(1,443–1,513)	2	0.1	(0.06–0.1)	2	11.8	(7.9–15.8)
	T&W	4	2,257	(928–4,429)	2	2.0	(0.2–3.8)	2	89.8	(35.9–143.8)
Total		110	4,631	(180–34,151)	108	22.4	(0.002–455.8)	94	45.3	(0.5–1699.9)
Atmospheric equilibrium			437	(371–609)		0.005	(0.002–0.05)		5.4	(0.5–13.2)

Notes. "Mainstem" represents means of the three mainstem reaches. Significant differences among the three mainstem reaches and T&W within each basin at $P < 0.05$ are indicated by different letters (ANOVA on rank followed by Dunn's test). Data of the Mekong upper reach ($n = 1$) and the Yellow River reaches ($n = 2$–5) were excluded from the statistical analysis.

Abbreviations: ANOVA, analysis of variance; ND, no data.

and lower reaches revealed the highest values of pCO_2 (up to 27,290 μatm), CH_4 (234.8 μM), and N_2O (1,699.9 nM) in the Ganges basin (Figure 4; Table 1). The lower reaches, consisting of the distributaries Hooghly and Padma, also flow along megacities (Kolkata and Dhaka), but exhibited lower levels of pCO_2 than the middle reaches. Similar patterns were observed for the concentrations of CH_4 and N_2O in the lower reaches.

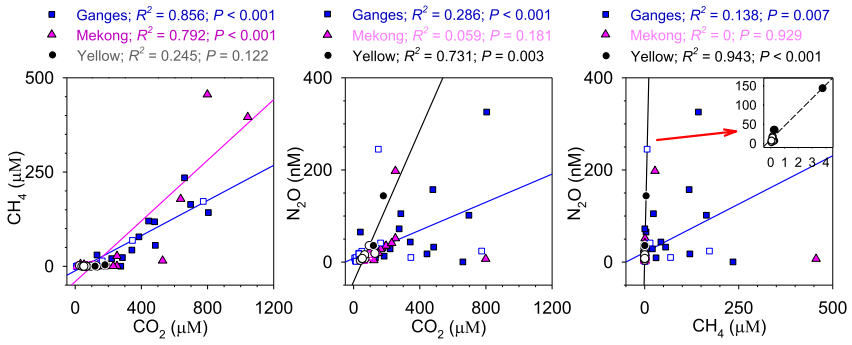

Figure 2. Relationships between the concentrations of CO_2, CH_4, and N_2O in the Ganges ($n = 52$–53), Mekong ($n = 32$–45), and Yellow River ($n = 9$–13). Significant relationships are indicated by regression lines. Void symbols indicate mainstem sites, while filled symbols represent tributaries and wastewater drains (T&W). The CH_4-N_2O regression in the Yellow River is shown in an inset box for a clearer view. An outlier of the Ganges data (N_2O: 1699.9 nM) was excluded from the regression analysis.

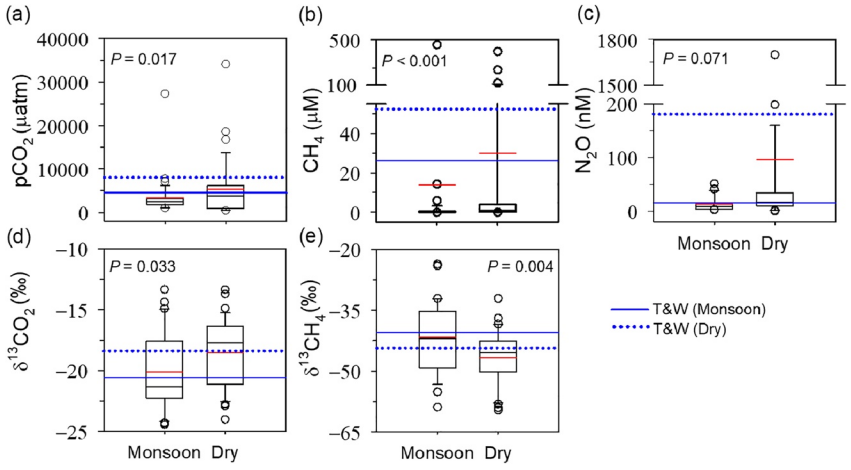

Figure 3. Seasonal comparison of pCO_2 (a), CH_4 (b), and N_2O concentrations (c), and $\delta^{13}C$ in CO_2 (d) and CH_4 (e) measured in the Ganges, Mekong, and Yellow River basins. The monsoon and dry season data from all sites (n = 26–35) are presented in boxplots, while the blue lines represent average values in tributaries and wastewater drains (T&W; n = 12–17). Significant seasonal differences are indicated by P values from Wilcoxon signed-rank test.

3.1.3. The Mekong River

The upper reach in the Tibetan Plateau with low population density showed lower values of pCO_2 (1,552 µatm) and CH_4 concentration (0.01 µM) than those found in the middle and lower reaches of the Mekong (Figure S1; Tables 1 and S2). The middle and lower reaches exhibited similar average levels of pCO_2 (2,379 and 2,325 µatm); however, the lower reach with a large discharge exhibited a wider range of pCO_2 (433–3,729 µatm) compared to the middle reach (1,384–2,948 µatm). Large variations in discharge along the lower reach (1,410–32,931 $m^3\ s^{-1}$; Li et al., 2013) can account for the large seasonal variability in pCO_2 with very low dry-season values approaching atmospheric equilibrium (Figure S1). N_2O concentrations were also similar across the middle and lower reaches. However, CH_4 concentrations averaged 0.3 µM in the lower reach, much higher than the concentrations observed in the middle reach. T&Ws along the middle and lower reaches showed the highest mean pCO_2 (7,536 µatm) (Figure S1; Table 1). CH_4 concentrations in T&W averaged 45.5 µM, which is 190 times higher than that of the mainstem average (0.2 µM). N_2O concentrations in T&W averaged 30.5 nM, which is three times higher than that of the mainstem average (9.8 nM).

3.1.4. The Yellow River

The Yellow River also exhibited supersaturation of CO_2 (694–4,861 µatm) and CH_4 (0.06–3.8 µM) across the basin (Figure S2; Table 1). Although the mean concentrations of CO_2 and CH_4 were lowest in the Yellow River, the mean N_2O concentration was 30.8 nM, higher than that of the Mekong (Table S3). The regressions between N_2O and CO_2 or CH_4 were significant, with a steeper slope than those of the Ganges and Mekong (Figure 2). The higher concentrations of N_2O corresponded to higher concentrations of PON and DIN in the basin, particularly along the middle reach (Figures 5e and 5f). In the middle reach, which traverses the metropolitan Hohhot and the Loess Plateau, the mean pCO_2 (2,475 µatm) and N_2O concentrations (14.7 nM) were highest in the basin, whereas the highest CH_4 concentrations were observed in the upper reach flowing through large areas of wetlands (Figure S2; Table 1).

3.2. Organic Matter Characteristics and Other Water Quality Parameters

Similar to the trends in the concentrations of the three GHGs, OM and other water quality parameters varied greatly between the three reaches and T&W in all three river basins (Figure 5). The concentrations of DOC in the mainstems of the three rivers spanned up to two orders of magnitude, with higher values found along the middle and lower reaches (Figure 5a). The mean DOC concentration at the T&W sites (6.5 mg L^{-1}) was ~3 times higher than that of the mainstems (2.4 mg L^{-1}). Similarly, the mean concentrations of POC, PON, and DIN in T&W were 4, 3, and 2 times higher than the corresponding concentrations

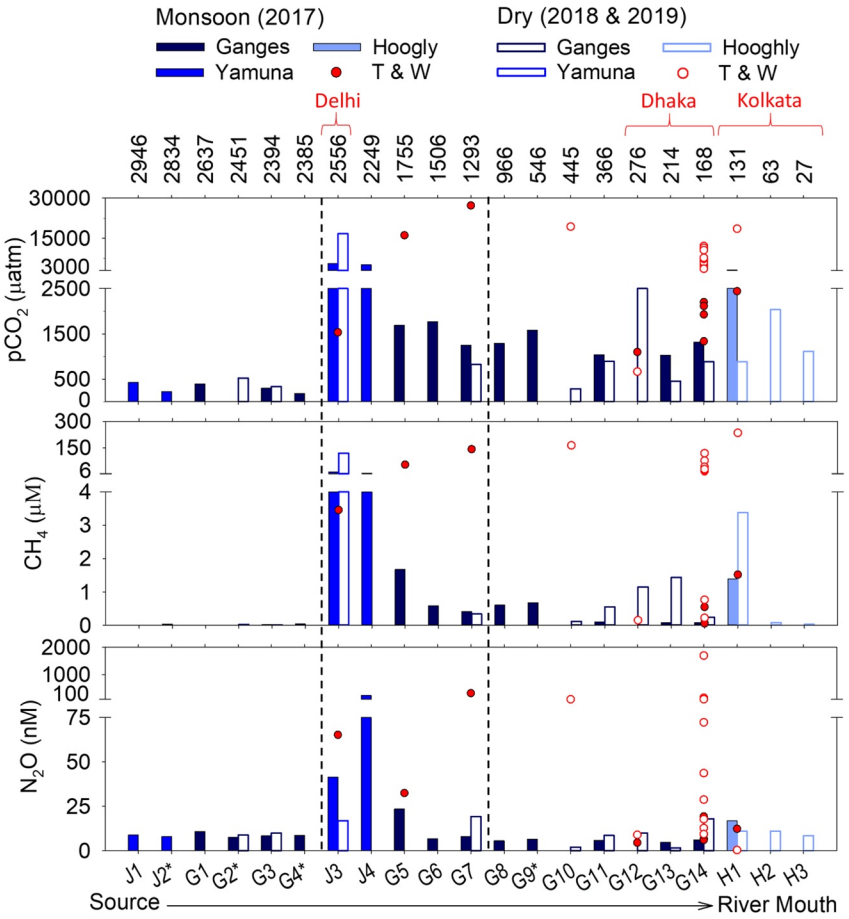

Figure 4. Longitudinal variations in pCO_2, and CH_4 and N_2O concentrations in the Ganges River basin. Main branches ("mainstem") shown in blue bars with different shades include the Ganges and Yamuna along the upper and middle reaches and the Hooghly and Padma along the lower reaches. Tributaries and wastewater drains (T&W) are shown in red circles with filled symbols for the monsoon and void symbols for the dry season. Upper, middle, and lower reaches are demarcated by dashed vertical lines, and samples from impounded sites are indicated by asterisks on site labels. The locations of three megacities in the Ganges basin are indicated on top of the figure.

in the mainstems (Figures 5d–5f). POC and PON concentrations were higher in the middle reaches (Figures 5d and 5e), consistent with the localized peaks of GHG concentrations (Figures 4, S1, and S2; Table 1).

Three identified PARAFAC components, including C1, C2, and C3, corresponded to humic-like, microbial humic-like, and protein-like fluorescence peaks, respectively (Figure S3; Begum et al., 2019; Fellman et al., 2010). The intensity of FDOM components, relative to the total fluorescence, displayed distinct spatial patterns across the mainstem reaches and T&W. Higher values of C3 were found along the middle and lower reaches of the Ganges and Yellow River, whereas C3 levels in the Mekong varied little, reflecting the small variation in DOC concentration (Figures 5a and 5c). The values of FI in the middle and lower reaches of the Ganges averaged 1.5 and 1.4, respectively, reflecting the contribution from wastewater-derived DOM with a mean FI value of 1.4 (Figure 5b).

The results of PCA showed that the two main components accounted for 60% of the total variance (Figure S4). The data were grouped into clusters of similar patterns and characteristics unique to each river basin, season, and four site categories (Figure S4). The samples from the upper and lower reaches were clustered in a small area associated with DOM optical indices including HIX, C1, C2, $SUVA_{254}$ (Figures S4a and S4d). On the other hand, overlapping clusters of the middle reaches and T&W were associated with the three GHGs, NH_4^+, PO_4^-, FI, and C3 (Figures S4a and S4d). The Yellow River cluster was distinguished from those of the Ganges and Mekong (Figure S4b), while the monsoon and dry-season clusters were also

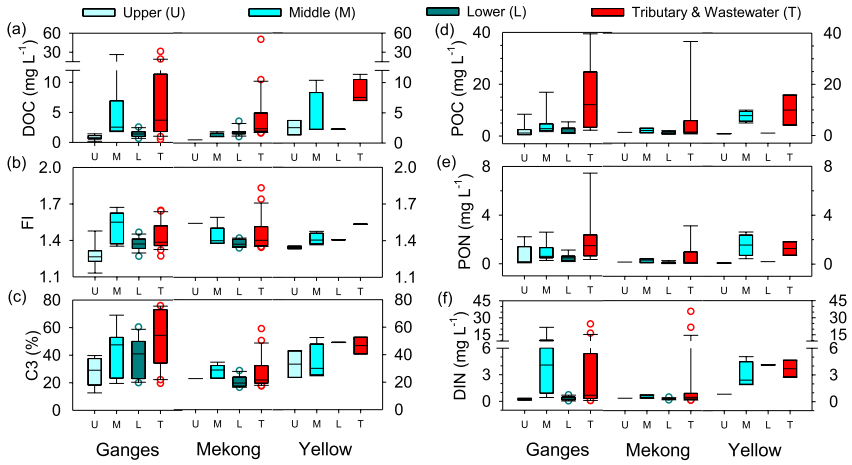

Figure 5. Inter-reach variations in dissolved organic carbon (DOC) (a), fluorescence index (FI) (b), C3 (c), particulate organic C (POC) (d), particulate organic N (PON) (e), and dissolved inorganic N (DIN) (f) in the Ganges (n = 29–53), Mekong (n = 19–45), and Yellow River (n = 9–12). "U," "M," "L," and "T" denote upper, middle, and lower reaches, and tributaries and wastewater drains, respectively.

discernable (Figure S4c). Regression analyses revealed significant positive relationships between GHG concentrations and other measurements including DOC, POC, PON, C3, FI, DIN, and PO_4^- (Figures 6, S5–S7). In contrast, the concentrations of GHGs exhibited significant negative relationships with C1, C2, DO, and pH for both the mainstems and T&W. The coefficients of correlation (R) were higher for CO_2 and CH_4 than N_2O.

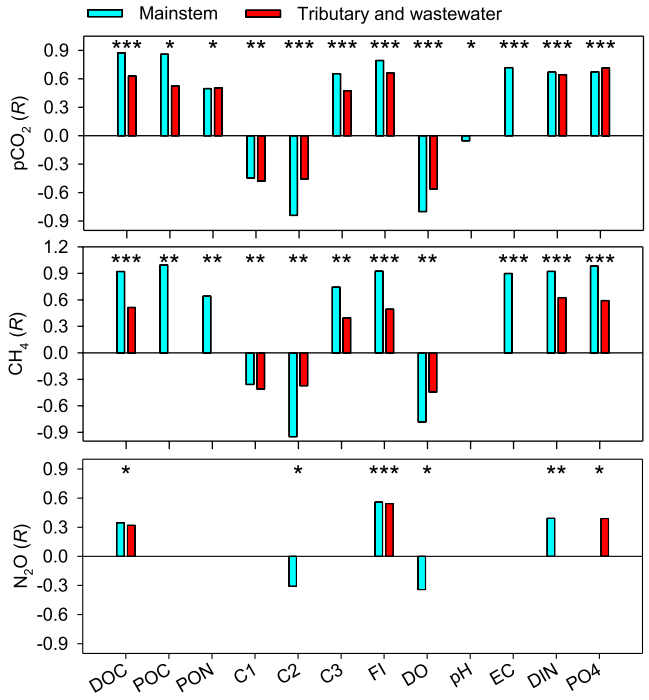

Figure 6. Significant relationships (R) between greenhouse gas concentrations (CO_2, CH_4, and N_2O) and the concentrations and optical properties of dissolved organic matter or other water quality parameters measured in the Ganges, Mekong, and Yellow River. Only significant relationships are shown with significance levels indicated by asterisks: * ($P < 0.05$), ** ($P < 0.01$), and *** ($P < 0.001$). DO, dissolved oxygen; DOC, dissolved organic carbon; DIN, Dissolved inorganic N; EC, electrical conductivity; FI, fluorescence index; POC, particulate organic C; PON, particulate organic N.

3.3. Stable C Isotope Ratios of CO_2 and CH_4

The values of δ^{13}C-CO_2 in the upper reaches tended to be higher than those measured across the middle and lower reaches of the Ganges and Mekong (Table 2). Longitudinal variation was more pronounced in the Ganges and Mekong than in the Yellow River. The upper reaches of the Ganges showed ^{13}C-enriched CO_2 with an average δ^{13}C of −13.3‰, whereas δ^{13}C-CO_2 averaged −17.1 and −18.2‰ in the middle and lower reaches, respectively, which were close to the mean (−18.6‰) for the T&W sites (Table 2). In the Mekong River basin, δ^{13}C-CO_2 values gradually decreased from the upper reach in the Tibetan Plateau (−14.6‰) to the impounded middle reach (−17.0‰) and the more urbanized lower reach (−21.1‰) (Table 2). T&W sites in the basin also showed more depleted values, averaging −20.1‰ (Table 2). However, δ^{13}C-CO_2 values in the lowest reach along Cantho exhibited downstream increases during the dry season, reflecting the seasonal increases at the local T&W sites (Figure 7). Compared to the patterns found in the Ganges and Mekong, the δ^{13}C-CO_2 values in the Yellow River showed less variation across the reaches (Table 2).

Complex patterns were observed for δ^{13}C-CH_4, with contrasting trends of enrichment (Ganges) and depletion (Yellow River) in ^{13}C from the upper to middle and lower reaches (Table 2). While the upper Ganges displayed the lowest value of δ^{13}C-CH_4 (−53.6‰), those of the middle reaches averaged −46.2‰, comparable to the average value of the T&W (−46.9‰); this result is consistent with the spatial patterns of the gas concentrations (Tables 1 and 2). In contrast, δ^{13}C-CH_4 in the middle and lower reaches of the Yellow River showed more negative values (−48.8 and −50.6‰) than the upper reach (−44.5‰), consistent with the high CH_4 concentrations

Table 2
Means and Ranges (Minimum–Maximum) of $\delta^{13}C$ in CO_2 and CH_4 Along the Upper, Middle, and Lower Reaches and Tributary and Wastewater Drains (T&W) in the Ganges, Mekong, and Yellow River

		$\delta^{13}C\text{-}CO_2$ (‰)			$\delta^{13}C\text{-}CH_4$ (‰)		
River	Reach	*n*	Mean	Range	*n*	Mean	Range
Ganges	Upper	8	−13.3[a]	(−20.8 to −6.0)	8	−53.6[a]	(−60.4 to −50.9)
	Middle	9	−17.1[b]	(−20.7 to −15.4)	9	−46.2[b]	(−50.3 to −41.2)
	Lower	14	−18.2[b]	(−22.9 to −12.6)	10	−49.6[ab]	(−59.1 to −34.7)
	T&W	22	−18.6[b]	(−24.3 to −13.7)	20	−46.9[b]	(−54.2 to −37.4)
	Basin	53	−17.5	(−24.3 to −6.0)	47	−48.5	(−60.4 to −34.7)
Mekong	Upper	1	−14.6		1	−42.3	
	Middle	5	−17.0[a]	(−20.2 to −14.4)		ND	
	Lower	14	−21.1[b]	(−24.3 to −16.0)	14	−44.0[a]	(−59.7 to −24.1)
	T&W	25	−20.1[ab]	(−24.5 to −13.3)	24	−41.4[a]	(−55.2 −23.7)
	Basin	45	−19.9	(−24.5 to −13.3)	39	−42.4	(−59.7 −23.7)
Yellow	Upper	2	−18.3	(−20.4 to −16.2)	2	−44.5	(−45.3 −43.7)
	Middle	5	−18.4	(−21.5 to −15.0)	3	−48.8	(−55.6 −40.2)
	Lower	2	−16.6	(−17.3 to −15.8)	2	−50.6	(−52.4 to −48.9)
	T&W	2	−18.9	(−20.1 to −17.8)	2	−40.4	(−48.7 to −32.1)
	Basin	11	−18.2	(−21.5 to −15.0)	9	−46.4	(−55.6 to −32.1)
Total		109	−18.5	(−24.5 to −6.0)	95	−45.8	(−60.4 to −23.7)

Notes. Significant differences among the three mainstem reaches and T&W within each basin at $P < 0.05$ are indicated by different letters (ANOVA on rank followed by Dunn's test). A few data of the Mekong upper reach ($n = 1$) and the Yellow River ($n = 2$–5) were excluded from the statistical analysis.
Abbreviations: ANOVA, analysis of variance; ND, no data.

along the upper reach (Tables 1 and 2). Given the lack of data for the middle reach of the Mekong, it is difficult to assess the basin-scale pattern for $\delta^{13}C\text{-}CH_4$. The $\delta^{13}C\text{-}CH_4$ values averaged −43.9‰ in the lower reach, similar to the measurement in the upper reach (−42.3‰). However, the wide range of $\delta^{13}C\text{-}CH_4$ in the lower reach was similar to the range observed for the T&W sites in the Mekong River basin (Figure 7; Table 2). In contrast to the dry-season increases in $\delta^{13}C\text{-}CO_2$ in the lowest reach, $\delta^{13}C\text{-}CH_4$ was significantly lower at both the mainstem and T&W sites during the dry season (Figure 7).

Although no significant relationship was found in the Keeling plot, the regressions in Miller-Tans plots were significant for both CO_2 and CH_4 when data were plotted for each river basin (Figure 8; Table S4). The slopes of the regressions for $\delta^{13}C\text{-}CO_2$ in the Ganges and Mekong were less steep (−16.7‰) than that for $\delta^{13}C\text{-}CO_2$ in the Yellow River (−18.5‰). In the regression models for $\delta^{13}C\text{-}CH_4$, the Ganges and Mekong showed more negative slopes (−48.3 and −44.8‰, respectively) than the Yellow River (−33.5‰). Significantly higher values of $\delta^{13}C\text{-}CO_2$ during the dry season were consistent with the seasonality found for the gas concentrations, whereas the opposite pattern was observed for the significantly lower values of $\delta^{13}C\text{-}CH_4$ during the dry season (Figure 3; Table S4). T&W sites exhibited higher values of $\delta^{13}C\text{-}CO_2$ (−16.1‰) and $\delta^{13}C\text{-}CH_4$ (−45.4‰) than the mainstems (−17.2 and −49.1‰). As indicated by the slopes of the Miller-Tans plots for CO_2, there was no clear difference in the origin of CO_2 between the rivers (Figure 8b); however, there was a noticeable difference in the slope for CH_4 between the Yellow River and the other basins (Figure 8d).

4. Discussion

4.1. Reach-Specific Patterns and Controls of CO_2, CH_4, and N_2O

The mean pCO_2 measured in the three river basins (4,631 μatm; Table 1) was much higher than the published global average riverine pCO_2 (2,400–3,100 μatm; Lauerwald et al., 2015; Raymond et al., 2013). The

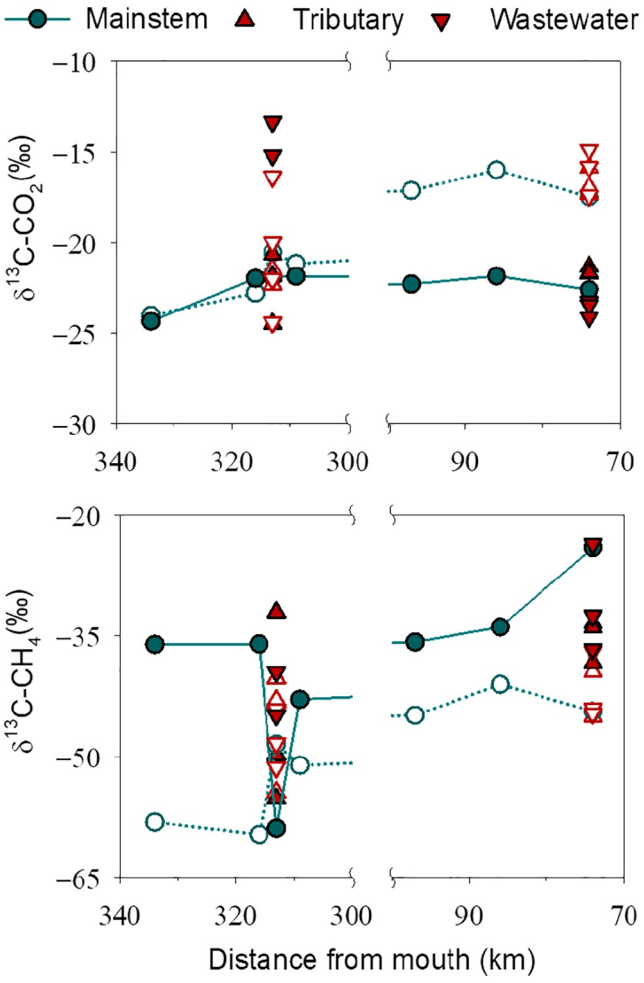

Figure 7. $\delta^{13}C$ in CO_2 and CH_4 in the lower reach of the Mekong, and urban tributaries and wastewater drains from Phnom Penh, Cambodia (334 km) and Can Tho, Vietnam (97 km from the river mouth). Dry and monsoon seasons are indicated by void and filled symbols, respectively.

mean pCO_2 in the Ganges (4,782 μatm) and Mekong (5,209 μatm) were 4–5 times higher than the earlier measurements summarized in Table S3 (Li et al., 2013; Lin et al., 2019; Park et al., 2018). These large differences might be ascribed to inaccuracy in previous pCO_2 measurements or estimates based on water quality parameters, that is, pH, temperature, and total alkalinity (Table S3; Li et al., 2013; Manaka et al., 2015). While some estimation-based studies were conducted on the basin scale, direct measurements were usually conducted for relatively short stretches of the rivers (Table S3; Alin et al., 2011; Cheng et al., 2019; Qu et al., 2017; Tian et al., 2019). In contrast, our field measurements in both the monsoon and dry seasons cover the entire basin including highly polluted tributaries and affected mainstem reaches. The levels of pCO_2, CH_4, and N_2O observed in the Ganges and Mekong exceed a few previously reported values (Li et al., 2013; Rao & Sarma, 2017; Rao et al., 2013; Park et al., 2018). The magnitude of the observed range of pCO_2 in the Yellow River basin (694–4,861 μatm; Table 1) is comparable to the reported values of pCO_2 measured along the upper reach (181–2,441 μatm; Qu et al., 2017; Tian et al., 2019) and across the basin (147–36,790 μatm; Ran et al., 2015). However, CH_4 concentrations observed in the upper reach (1.0 μM) of the Yellow River were much higher than the reported value (0.02 μM; Qu et al., 2017). While there have been some reports on pCO_2 (Samanta et al., 2015; Sarma et al., 2012), CH_4 concentrations (Rao & Sarma, 2017), and N_2O concentrations (Rao et al., 2013) in the Ganges estuaries and coastal areas (Table S3), only a few studies reported pCO_2 calculated from water quality measurements in headwater streams (Chakrapani & Veizer, 2005; Park et al., 2018) or the lower Ganges in Bangladesh (Manaka et al., 2015). Our basin-wide measurements of pCO_2 across the Ganges (180–27,290 μatm) far exceeded the range of reported values (65–2,620 μatm; Table S3). The ranges of CH_4 (0.03–3.4 μM) and N_2O concentrations (1.7–18.1 nM) in the lower reaches (Table 1) also exceed the previous measurements in the estuary and coastal area (Table S3; Rao & Sarma, 2017; Rao et al., 2013).

The highest value of pCO_2 in the middle reach of the Ganges, downstream of Delhi (20,580 μatm; Figure 4), has never been reported for the Ganges basin. The large metropolitan populations discharging loads of untreated wastewater, up to $1{,}104 \times 10^6$ tons yr^{-1} in the case of Delhi (Table S2),

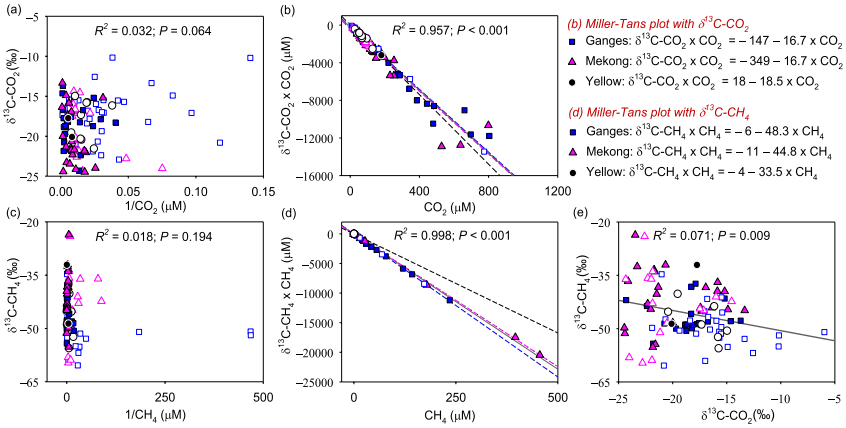

Figure 8. Keeling and Miller-Tans plots for $\delta^{13}C$-CO_2 (a and b) and $\delta^{13}C$-CH_4 (c and d) and the correlation between $\delta^{13}C$-CO_2 and $\delta^{13}C$-CH_4 (e). Significant regressions are indicated by dashed (each river) and solid lines (all data combined). Void and filled symbols represent mainstem, and tributaries and wastewater drains (T&W), respectively.

may represent the primary anthropogenic perturbation to the production and consumption of GHGs in the Ganges. Untreated and poorly treated wastewater generated from the ever-expanding population centers in India and Bangladesh can greatly impact downstream water quality by inducing surges in biochemical oxygen demand (BOD) and nutrients (CPCB 2013, Park et al., 2018; Sharma et al., 2017). Although reach-specific data on wastewater is not available, the longitudinal patterns of GHGs in the Mekong and Yellow River can also be explained by increasing volumes of wastewater generated along the middle and lower reaches (Tables 1 and S2). Riparian countries along the lower Mekong River generate large volumes of wastewater ranging from 17 (Myanmar) to 5,293 $\times$ 10^6 tons yr^{-1} (Thailand) (Table S2), and a large fraction of the wastewater enters the river untreated (Park et al., 2018; Sato et al., 2013). The Chinese provinces in the Yellow River basin produce wastewater ranging from 271 to 4,999 $\times$ 10^6 tons yr^{-1} (Table S2); however, ~90% of the total wastewater in China is treated before discharging into the rivers (Table S2; China Statistical Yearbook, 2018; Qi et al., 2020). The relatively high rate of wastewater treatment in the Yellow River is partially responsible for the comparatively low concentrations of CO_2 and other GHGs, because untreated wastewater can produce significantly higher amounts of CO_2 than treated wastewater (Kim et al., 2019).

Increased loads of BOD and nutrients from wastewater can enhance the riverine production of CO_2 and other GHGs via photo- and biodegradation of OM in the water column and anaerobic metabolic processes at the benthic sediment (Begum et al., 2019; Kim et al., 2019; Yoon et al., 2017). Significant positive relationships between the concentrations of the three GHGs and C3, FI, DIN, and PO_4^-, respectively, suggest that the degradation of wastewater-derived OM in eutrophic rivers may represent a major source of riverine GHGs (Figure 6). Strong correlations between GHG concentrations and C3 (protein-like fluorescence) or FI also indicate the production of labile OM (Ulliman et al., 2020) and GHGs from wastewater effluents (Jin et al., 2018). Similar to the positive priming effect of labile OM on recalcitrant DOM in rivers (Bianchi et al., 2015), a synergistic increase in CO_2 and other GHG concentrations was observed when wastewater was mixed with reservoir or impounded river water (Begum et al., 2019; Wang et al., 2017).

Polluted sites along the urbanized mainstems and T&W exhibited high concentrations of CH_4 and N_2O, proportional to the concentrations of CO_2, which was consistent with positive correlations between GHGs (Figure 2). Large emissions of CH_4 and N_2O from treated wastewater effluents in downstream reaches have also been measured in other urbanized river systems of Asia (Jin et al., 2018; Li et al., 2020) and Europe (Alshboul et al., 2016). Wastewater effluents are rich in OM but depleted in DO, providing favorable conditions for the production of CH_4 through anaerobic biodegradation (Alshboul et al., 2016; Li et al., 2020). Low concentrations of DO in T&W also allow for high concentrations of CH_4 by limiting oxidation of the produced CH_4 (Li et al., 2020). The oxidation of CH_4 in water column has been suggested as the major pathway for CH_4 removal in the Amazon (Sawakuchi et al., 2016) and Han River (Jin et al., 2018). Higher concentrations of NO_3^- in wastewater can increase N_2O concentrations in the T&W and polluted middle and lower reaches of the studied rivers (Figure 5; Table 1) through denitrification under anoxic or hypoxic conditions (Beaulieu et al., 2010; Jin et al., 2018). Although denitrification is considered the predominant pathway for N_2O production in the river, oxic and hypoxic conditions with higher concentrations of NH_4^+ can facilitate N_2O production via nitrification and nitrifier-denitrification, respectively (Beaulieu et al., 2010; Li et al., 2020).

Higher mean concentrations of CO_2, CH_4, and N_2O during the dry season (Figure 3) are consistent with the seasonal patterns found in other polluted rivers (Jin et al., 2018; Li et al., 2020; Wang et al., 2017; Yoon et al., 2017). Higher dry-season GHG concentrations can be explained by the fact that wastewater influence on downstream water quality is stronger during the dry season, whereas increased flows induce a greater dilution effect during the monsoon season. Dry-season increases in GHG concentrations were observed in polluted reaches of the Han River in Korea, where wastewater accounted for ~5% and 12% of the mainstem river flow in the monsoon and dry season, respectively (Jin et al., 2018; Yoon et al., 2017). Lower GHG concentrations during the monsoon period (Figure 3) might have resulted from wastewater dilution by a monsoonal increase in discharge. However, higher concentrations of GHGs observed in several sites along the middle and lower reaches of the studied rivers (Figures 4, S1, and S2) are consistent with the patterns of pCO_2 observed in some sites of the lower Mekong (Borges, Abril, & Bouillon, 2018; Li et al., 2013) and the lower Yellow River (Ran et al., 2015). Monsoonal increases in CO_2 have been explained by the flushing of CO_2 and OM from the soil, floodplains, and other allochthonous sources and subsequent degradation of the allochthonous OM during riverine transport (Borges, Abril, & Bouillon, 2018; Li et al., 2013).

Very low dry-season pCO_2 found in some mainstem sites of the three rivers (Figures 4, S1, and S2) may indicate an enhanced primary production consuming dissolved CO_2. Deviating from the mean DO values of 5.6 (dry) and 6.1 mg L^{-1} (monsoon), these sites exhibited higher concentrations of DO during the dry season when additional O_2 was produced via primary production (Figure S5). Since primary production through photosynthesis and microbial respiration are concurrent processes in the aquatic system, a small change in an environmental variable, for example, nutrients, DO, and DOC concentration, can transform the system from a heterotrophic source of CO_2 to an autotrophic sink (Wang et al., 2017).

4.2. Impacts of Local Pollution on GHGs and C Isotope Ratios

While $\delta^{13}C$ has widely been measured to track downstream alterations of various DIC components in inland water systems, including CO_2, HCO_3^-, and CO_3^{2-} (Borges, Abril, & Bouillon, 2018; Campeau et al., 2017; Jin et al., 2018), our approach is unique in linking the optical characterization of wastewater-derived DOM to the isotopic signatures of CO_2 and CH_4 in the urbanized middle and lower reaches of the studied rivers. The measured values of $\delta^{13}C$-CO_2 ranging from −6.0 to −24.5‰ (Table 2) span nearly the full range of reported values of $\delta^{13}C$-CO_2 in streams, rivers, and estuaries (Campeau et al., 2017; Jin et al., 2018; Maher et al., 2013; McCallister & del Giorgio, 2008). The relatively high $\delta^{13}C$-CO_2 values, up to −6.0‰, in the upper reaches of the Ganges (Table 2) were similar to the level of ^{13}C enrichment in DIC (−16.8 and −5.2‰) observed in the headwater streams of the Ganges (Chakrapani & Veizer, 2005), indicating the geogenic origins of the gas. Significant decreases in $\delta^{13}C$-CO_2 from the upper to the middle and lower reaches of the Ganges imply increasing contributions from biogenic (i.e., plant-derived soil OM) and anthropogenic (wastewater) sources along the polluted reaches (Campeau et al., 2017; Jin et al., 2018). Reported values of ^{13}C-DIC range from −27 to −18‰ for biogenic sources (Campeau et al., 2017; Jin et al., 2018) and from −13.7 to −10.1‰ for wastewater effluents (Yang et al., 2018).

Similarly, longitudinal decreases in $\delta^{13}C$-CO_2 along the Mekong indicate an increasing contribution of ^{13}C-depleted CO_2 from soils and wastewater OM along the lower reaches (Campeau et al., 2017). In contrast, the more negative values of $\delta^{13}C$-CO_2 in the upper reaches of the Mekong and Yellow River (Table 2) than those of the Ganges suggest a contribution from natural wetlands (Avery et al., 1999; Qin et al., 2020). Large expanses of natural wetlands are scattered across the source regions of the rivers deriving from the Qinghai-Tibetan Plateau (Tong et al., 2014). Despite the differences in the background levels observed in the upper reaches, $\delta^{13}C$-CO_2 values lower than −12.6‰ in the middle and lower reaches of the three rivers reveal anthropogenic impacts on the downstream deviations from the headwater isotopic signatures reflecting geogenic origins (Table 2). The shifting values of $\delta^{13}C$-CO_2 along the middle and lower reaches may reflect the combined effects of allochthonous contributions from soils (Campeau et al., 2017; Doctor et al., 2008) and wastewater (Jin et al., 2018; Li et al., 2020) as well as concurrent instream processes such as DOM mineralization (McCallister & del Giorgio, 2008), primary production (Alling et al., 2012), and anaerobic metabolic processes in the benthic sediments (Barth et al., 2003).

The values of $\delta^{13}C$-CO_2 observed at the T&W sites of the three rivers (−24.5 to −13.3‰) were similar to the values observed in other urbanized Asian rivers (−18.3 to −14.7‰; Jin et al., 2018), but lower than the values of $\delta^{13}C$-DIC measured in rivers (−12.9 to −11.0‰; Li et al., 2020) and WWTP effluents (−13.7 to −10.1‰; Yang et al., 2018). These values of $\delta^{13}C$ in CO_2 and DIC found in wastewater and downstream rivers indicate ^{13}C depletion or enrichment in CO_2 compared with the isotopic signatures of geogenic or biogenic sources, respectively. The magnitude of ^{13}C enrichment relative to the biogenic source is greater in the Ganges and Mekong than in the Yellow River (Figure 8b; Tables 2 and S4), which can be explained by the fact that the latter is less loaded with untreated wastewater (Park et al., 2018; Qi et al., 2020). These variations in $\delta^{13}C$-CO_2, along with the differences in regression slopes of the Miller-Tans plots (Figure 8b; Table S4), reflect the impact of the larger amounts of CO_2 derived from the untreated wastewater and highly polluted tributaries of the Ganges and Mekong, compared to those derived from treated wastewater effluents in the Yellow River (CPCB, 2013; Qi et al., 2020).

Significantly higher concentrations of CO_2 in the dry season (Figure 3a) were reflected in the less negative values of $\delta^{13}C$-CO_2 (−18.5‰), compared to those found in the monsoon season (−20.1‰) (Figure 3d). These enriched values of $\delta^{13}C$-CO_2 in streams and rivers have often been attributed to natural processes such as atmospheric evasion and instream primary production, both of which can preferentially remove the lighter

isotope from the river DIC pool (Alling et al., 2012; Campeau et al., 2017; Doctor et al., 2008). Therefore, CO_2 outgassing can result in significant ^{13}C-enrichment of stream CO_2 and DIC; for instance, Doctor et al. (2008) reported a 3–5‰ increase in $\delta^{13}C$-DIC in a forested headwater stream owing to atmospheric evasion. Photosynthesis can also increase $\delta^{13}C$-CO_2; for example, Jin et al. (2018) reported concomitant increases in Chlorophyll *a* and $\delta^{13}C$-CO_2 along the polluted tributaries and eutrophic lower reach of the Han River, Korea. The enrichment of ^{13}C in CO_2 can also reflect contributions of CO_2 from microbial OM degradation in wastewater drains and polluted tributaries during the dry season (Jin et al., 2018; Li et al., 2020). The less negative slope of $\delta^{13}C$-CO_2 in the Miller-Tans plot in T&W (−16.1‰), compared to the more negative slope in the mainstems (−17.2‰) may suggest that wastewaters are a major source of such enrichment (Table S4).

The enrichment of ^{13}C in CO_2 and depletion of ^{13}C in CH_4 in the dry season (Figures 3d and 3e) also reflect the reduction of CO_2 in the benthic sediment under anoxic conditions (Barth et al., 2003; Jin et al., 2018; Qin et al., 2020). Similarly, CH_4 produced in the sediment through hydrogenotrophic methanogenesis (CO_2 reduction) might explain the more negative $\delta^{13}C$-CH_4 observed during the dry season (−46.8‰) than during the monsoon season (−41.7‰) (Figure 3e; Qin et al., 2020). However, active CH_4 oxidation in oxic waters has been proposed as the prevailing mechanism of ^{13}C-CH_4 enrichment during the high-flow periods, resulting in the production of ^{13}C-depleted CO_2 (Jin et al., 2018; Maher et al., 2013; Sawakuchi et al., 2016). This seasonal shift from enriched ^{13}C-CO_2 during the dry season to enriched ^{13}C-CH_4 during the monsoon season was observed along the short stretch of the river in the Mekong delta (Figure 7). The drastic monsoonal decline in $\delta^{13}C$-CH_4 downstream of an urban tributary along the lower reach of the Mekong (−36.0 to −58.9‰; Figure 7) was similar to the patterns observed in the reaches of the Han River (Jin et al., 2018) and Seine River (Garnier et al., 2013) that receive loads of WWTP effluents. The lower dry-season values of $\delta^{13}C$-CH_4 increased gradually along the lower reach of the Mekong River (Figure 7), contrasting with decreases in CH_4 concentration (Figure S1). This suggests efficient removal of CH_4 through oxidation and/or atmospheric evasion (Jin et al., 2018; Maher et al., 2013; Sawakuchi et al., 2016).

The unusually high CH_4 concentration in the upper reach of the Yellow River (Figure S2) may be associated with ^{13}C enrichment in CH_4 (Table 2), consistent with reported values in peatlands (Avery et al., 1999; Qin et al., 2020). Avery et al. (1999) reported that ∼84% of CH_4 in the Michigan peatland was produced by acetoclastic methanogenesis with $\delta^{13}C$-CH_4 values averaging −48.7‰ in the summer. Impounded sites also showed depleted values of $\delta^{13}C$-CH_4 ranging from −51.4 to −60.5‰ in the Ganges during the dry season, which were similar to the value (−57.8‰) observed in the Qinghai Lake located 102 km away from site Y2 (data obtained from the field trip to the upper Yellow River). Previous studies in Tuojia River (Qin et al., 2020), Arctic tundra watersheds (Throckmorton et al., 2015), and the Michigan peatland (Avery et al., 1999) have reported seasonal shifts in production pathways of CH_4 from hydrogenotrophic methanogenesis prevailing in the winter to acetoclastic methanogenesis in summer. O'Dwyer et al. (2020) linked CH_4 production in Alaskan lakes during the winter season to ecosystem productivity. Lower values of $\delta^{13}C$-CH_4 from hydrogenotrophic methanogenesis were observed in productive lakes rich in biodegradable OM, compared to the values associated with acetolactic methanogenesis occurring in anoxic systems rich in recalcitrant, aromatic OM (O'Dwyer et al., 2020). Thus, enhanced CH_4 oxidation and atmospheric evasion in the monsoon and reduction of CO_2 in anoxic water during dry season may result in seasonal shifts in $\delta^{13}C$ enrichment in CH_4.

4.3. Implications for Regional and Global Riverine GHG Budgets

Interbasin differences in riverine DOM properties and GHG concentrations suggest the strong influence of watershed management and wastewater treatments on riverine GHG emissions. Although this study focused on controlling mechanisms for the spatiotemporal variations in GHG concentrations, estimates based on published values of gas transfer velocity (*k*) (Lauerwald et al., 2015; Raymond et al., 2012) are briefly discussed here. Based on *k* values for large global rivers (Lauerwald et al., 2015), emissions of CO_2, CH_4, and N_2O from the studied rivers were estimated at 11.4–14.8, 2.0–2.7, and 8.0–10.4 mg N m^{-2} d^{-1}, respectively (Table S5). The estimated emission rates were higher than the reported riverine CO_2 emissions from the global (3.4–5.4 g C m^{-2} d^{-1}), tropical (3.0–9.7 g C m^{-2} d^{-1}), or temperate (1.4–4.7 g C m^{-2} d^{-1}) streams and rivers (Alin et al., 2011; Aufdenkampe et al., 2011; Lauerwald et al., 2015). The estimated CH_4 emission rates exceed the reported averages for the diffusive (0.10 g C m^{-2} d^{-1}) and ebullitive fluxes (0.02 g C m^{-2} d^{-1})

from the global rivers (Stanley et al., 2016). The N_2O emission estimates also surpass the wide range of global riverine N_2O emissions (−0.03–7.4 mg N m^{-2} d^{-1}) estimated by Hu et al. (2016). The observed high concentrations and fluxes of GHGs along the middle and lower reaches reflect the contributions of T&W, as illustrated by the high GHG emissions from T&W (Table S5). These localized increases in GHGs along the urbanized middle and lower reaches underscore the importance of incorporating anthropogenically impacted river reaches in the riverine GHG budgets. Extremely high concentrations of GHGs measured across the T&W sites can not only directly enter the receiving river but also emit to the atmosphere at 8–20 times higher emission rate (Table S5).

Individual anthropogenic perturbations have been shown to enhance riverine GHG fluxes on a regional and global scale (Deemer et al., 2016; Garnier et al., 2013; He et al., 2017; Li et al., 2020; Yoon et al., 2017). However, much less is known about the synergistic effect of impoundments and WWTP effluents on riverine GHG emissions. A few studies have reported an enhanced production of GHGs from the mixing of OM, nutrients, and microbial communities in eutrophic, impounded rivers (Begum et al., 2019; Wang et al., 2017). The potential enhancement of production of GHGs in impounded reaches was indicated by the increases in CH_4 and N_2O concentrations from M2 (dam) to M3 (downstream of Jinghong), while pCO_2 remained similar during the dry season (Figure S1). The significant relationships between GHG concentrations and DOC, POC, DIN, and the optical properties of DOM (Figures 6, S5–S7), respectively, suggest that the DOM pool fueling riverine heterotrophy may be continuously replenished by allochthonous DOM of natural or anthropogenic origin and autochthonous DOM produced in the eutrophic, impounded reaches.

Although long-term data are required to assess anthropogenic perturbations, we focused on providing field measurements as baseline data required to explore how longitudinally varying distributions of pollution sources affect both the spatial and seasonal variations in GHG concentrations along the three rivers. Anthropogenic alterations in the concentrations of GHGs and other biogeochemical constituents over a long period have often been assessed using modeling due to lack of field measurements (Regnier et al., 2013). Our approach includes finding anthropogenic footprints in DOM optical properties (Figure 5) and stable C isotopes of GHGs (Table 2; Figure 7) and then link them to GHG concentrations in the mainstem reaches and T&W (Figures 6 and 8). Despite the short span of this study, data from two contrasting hydrological conditions allowed for comparing variable effects of wastewater on the mainstem reaches. These results illustrated the importance and advantage of comparing seasonal data across the three years to investigate anthropogenic perturbations to the riverine dynamics of GHGs and DOM. Therefore, our multi-parameter comparison across the pre-defined spatiotemporal scales could form a framework for long-term future studies that can track the temporal evolution of anthropogenic impacts on GHG emissions from understudied large Asian rivers.

5. Conclusions

Spatiotemporal variations in CO_2, CH_4, and N_2O concentrations illustrate the strong localized influences of wastewater on the dynamics of the three GHGs in the urbanized reaches of the Ganges, Mekong, and Yellow River. The extremely high levels of GHGs found in the middle reaches of the Ganges far exceed the reported levels estimated from water quality data, which underscores the necessity of high-resolution field measurements in many understudied rivers across Asia. Seasonal variability in discharge plays a crucial role in controlling riverine GHG dynamics across the three basins; in the dry season, higher GHG emissions can occur along the reaches receiving high loads of wastewater. Both inter-reach and interbasin variations in GHGs and OM concentrations suggest that GHGs derived from anthropogenic sources can be emitted to the atmosphere within a short stretch, fueled by the degradation of anthropogenic DOM during downstream transport.

This study provides a rare field data set that encompasses the large spatiotemporal variations in three GHGs across the various reaches and tributaries of the three large rivers of Asia. These field-based data will be very useful for establishing regional budgets and policy responses to the rapidly increasing levels of water pollution and riverine GHG emissions. Very high GHG concentrations observed within short stretches downstream of metropolitan areas emphasize the importance of including such anthropogenically impacted reaches in riverine GHG budgets to provide emission estimates that reflect the rapid changes occurring in

increasingly urbanized river basins across Asia and worldwide. This requires a careful evaluation of anthropogenic alterations to riverine metabolic processes and associated increases in GHG emissions. Differences in natural watershed characteristics, population, wastewater discharge, urbanization, and impoundment need to be examined in more river systems in Asia and other understudied regions to better assess anthropogenic perturbations to global riverine emissions of GHGs. Our unique approach combining optical properties of DOM with stable C isotopes in CO_2 and CH_4 can be applied to explore the source and production mechanisms of GHGs in these river systems under increasing anthropogenic stresses. Despite the limited temporal coverage, the longitudinal variations in DOM properties and GHG concentrations suggested strong contributions of wastewater and polluted tributaries to the riverine C fluxes across the three river basins. These results can thus provide a baseline for scoping future studies that can further assess human impacts on GHG emissions from the three studied and other Asian rivers underrepresented in the global riverine C budgets.

Data Availability Statement

Additional details of Materials and Methods (Text S1), supplementary figures (Figures S1–S7), and supplementary tables (Tables S1–S5) are included in the Supporting Information. Data set for this research is available on PANGAEA (https://doi.org/10.1594/PANGAEA.926582), as detailed in the in-text data citation: Begum et al. (2021) (with CC-BY-4.0 license).

Acknowledgments
This work was supported by the Asia-Pacific Network for Global Change Research (CRRP2016-01MY-Park) and the National Research Foundation of Korea funded by the Korean Government (NRF-2017R1D1A1B06035179). The authors thank the students of Jahangirnagar University, Royal University of Phnom Penh, Cantho University, and University of Inner Mongolia for their assistance with sampling. The authors declare that they have no conflict of interest.

References

Abril, G., Martinez, J.-M., Artigas, L. F., Moreira-Turcq, P., Benedetti, M. F., Vidal, L., et al. (2014). Amazon River carbon dioxide outgassing fuelled by wetlands. *Nature*, *505*(7483), 395–398. https://doi.org/10.1038/nature12797

Alin, S. R., Rasera, M. D. F. F. L., Salimon, C. I., Richey, J. E., Holtgrieve, G. W., Krusche, A. V., & Snidvongs, A. (2011). Physical controls on carbon dioxide transfer velocity and flux in low-gradient river systems and implications for regional carbon budgets. *Journal of Geophysical Research*, *116*(1), G01009. https://doi.org/10.1029/2010JG001398

Alling, V., Porcelli, D., Mörth, C.-M., Anderson, L. G., Sanchez-Garcia, L., Gustafsson, Ö., et al. (2012). Degradation of terrestrial organic carbon, primary production and out-gassing of CO_2 in the Laptev and East Siberian Seas as inferred from $\delta^{13}C$ values of DIC. *Geochimica et Cosmochimica Acta*, *95*, 143–159. https://doi.org/10.1016/j.gca.2012.07.028

Alshboul, Z., Encinas-Fernández, J., Hofmann, H., & Lorke, A. (2016). Export of dissolved methane and carbon dioxide with effluents from municipal wastewater treatment plants. *Environmental Science & Technology*, *50*(11), 5555–5563. https://doi.org/10.1021/acs.est.5b04923

Aufdenkampe, A. K., Mayorga, E., Raymond, P. A., Melack, J. M., Doney, S. C., Alin, S. R., et al. (2011). Riverine coupling of biogeochemical cycles between land, oceans, and atmosphere. *Frontiers in Ecology and the Environment*, *9*(1), 53–60. https://doi.org/10.1890/100014

Avery, G. B., Shannon, R. D., White, J. R., Martens, C. S., & Alperin, M. J. (1999). Effect of seasonal changes in the pathways of methanogenesis on the $\delta^{13}C$ values of pore water methane in a Michigan peatland. *Global Biogeochemical Cycles*, *13*(2), 475–484. https://doi.org/10.1029/1999GB900007

Barth, J. A. C., Cronin, A. A., Dunlop, J., & Kalin, R. M. (2003). Influence of carbonates on the riverine carbon cycle in an anthropogenically dominated catchment basin: Evidence from major elements and stable carbon isotopes in the Lagan River (N. Ireland). *Chemical Geology*, *200*(3–4), 203–216. https://doi.org/10.1016/S0009-2541(03)00193-1

Bastviken, D., Tranvik, L. J., Downing, J. A., Crill, P. M., & Enrich-Prast, A. (2011). Freshwater methane emissions offset the continental carbon sink. *Science*, *331*, 50. https://doi.org/10.1126/science.1196808

Beaulieu, J. J., Shuster, W. D., & Rebholz, J. A. (2010). Nitrous oxide emissions from a large, impounded river: The Ohio River. *Environmental Science & Technology*, *44*, 7527–7533. https://doi.org/10.1021/es1016735

Begum, M. S., Bogard, M. J., Butman, D. E., Chea, E., Kumar, S., Lu, X., et al. (2021). *Spatiotemporal variation in pCO_2, CH_4, N_2O, DOM, and ancillary water quality measured in the Ganges, Mekong, and Yellow River during 2016 to 2019*. PANGAEA. https://doi.org/10.1594/PANGAEA.926582

Begum, M. S., Jang, I., Lee, J.-M., Oh, H. B., Jin, H., & Park, J.-H. (2019). Synergistic effects of urban tributary mixing on dissolved organic matter biodegradation in an impounded river system. *Science of the Total Environment*, *676*, 105–119. https://doi.org/10.1016/j.scitotenv.2019.04.123

Bianchi, T. S., Thornton, D. C. O., Yvon-lewis, S. A., King, G. M., Eglinton, T. I., Shields, M. R., et al. (2015). Positive priming of terrestrially derived dissolved organic matter in a freshwater microcosm system. *Geophysical Research Letters*, *42*, 5460–5467. https://doi.org/10.1002/2015GL064765

Borges, A. V., Abril, G., & Bouillon, S. (2018). Carbon dynamics and CO_2 and CH_4 outgassing in the Mekong delta. *Biogeosciences*, *15*(4), 1093–1114. https://doi.org/10.5194/bg-15-1093-2018

Borges, A. V., Darchambeau, F., Lambert, T., Bouillon, S., Morana, C., Brouyère, S., et al. (2018). Effects of agricultural land use on fluvial carbon dioxide, methane and nitrous oxide concentrations in a large European river, the Meuse (Belgium). *Science of the Total Environment*, *610–611*, 342–355. https://doi.org/10.1016/j.scitotenv.2017.08.047

Borges, A. V., Darchambeau, F., Teodoru, C. R., Marwick, T. R., Tamooh, F., Geeraert, N., et al. (2015). Globally significant greenhouse-gas emissions from African inland waters. *Nature Geoscience*, *8*(8), 637–642. https://doi.org/10.1038/ngeo2486

Butman, D., & Raymond, P. A. (2011). Significant efflux of carbon dioxide from streams and rivers in the United States. *Nature Geoscience*, *4*(12), 839–842. https://doi.org/10.1038/ngeo1294

Campeau, A., Wallin, M. B., Giesler, R., Löfgren, S., Mörth, C.-M., Schiff, S., et al. (2017). Multiple sources and sinks of dissolved inorganic carbon across Swedish streams, refocusing the lens of stable C isotopes. *Scientific Reports*, *7*(1), 1–14. https://doi.org/10.1038/s41598-017-09049-9

Chakrapani, G. J., & Veizer, J. (2005). Dissolved inorganic carbon isotopic compositions in the Upstream Ganga River in the Himalayas. *Current Science*, *89*(3), 553–556.

Cheng, F., Zhang, H.-M., Zhang, G.-L., Liu, S.-M., Song, G.-D., & Du, G.-X. (2019). Distribution and emission of N_2O in the largest river-reservoir system along the Yellow River. *Science of the Total Environment*, *666*, 1209–1219. https://doi.org/10.1016/j.scitotenv.2019.02.277

China Statistical Yearbook. (2018). *Compiled by the National Bureau of Statistics of China*. China Statistics Press. Retrieved from http://www.stats.gov.cn/tjsj/ndsj/2018/indexeh.htm

Cole, J. J., Prairie, Y. T., Caraco, N. F., McDowell, W. H., Tranvik, L. J., Striegl, R. G., et al. (2007). Plumbing the global carbon cycle: Integrating inland waters into the terrestrial carbon budget. *Ecosystems*, *10*(1), 172–185. https://doi.org/10.1007/s10021-006-9013-8

CPCB: Central Pollution Control Board. (2013). *Pollution assessment: River Ganga, Ministry of Environment and Forests, India*.

Deemer, B. R., Harrison, J. A., Li, S., Beaulieu, J. J., Delsontro, T., Barros, N., et al. (2016). Greenhouse gas emissions from reservoir water surfaces: A new global synthesis. *BioScience*, *66*(11), 949–964. https://doi.org/10.1093/biosci/biw117

Degens, E. T., Kempe, S., & Richey, J. E. (1991). Summary: Biogeochemistry of major world river. In E. T. Degens, S. Kempe, & J. E. Richey (Eds.), Biogeochemistry of major world rivers, SCOPE 42 (Vol. 15, pp. 323–347). J. Wiley & Sons.

Doctor, D. H., Kendall, C., Sebestyen, S. D., Shanley, J. B., Ohte, N., & Boyer, E. W. (2008). Carbon isotope fractionation of dissolved inorganic carbon (DIC) due to outgassing of carbon dioxide from a headwater stream. *Hydrological Processes*, *22*(14), 2410–2423. https://doi.org/10.1002/hyp.6833

Dutta, V., Dubey, D., & Kumar, S. (2020). Cleaning the River Ganga: Impact of lockdown on water quality and future implications on river rejuvenation strategies. *Science of the Total Environment*, *743*, 140756. https://doi.org/10.1016/j.scitotenv.2020.140756

Evans, A. E. V., Hanjra, M. A., Jiang, Y., Qadir, M., & Drechsel, P. (2012). Water quality: Assessment of the Current Situation in Asia. *International Journal of Water Resources Development*, *28*(2), 195–216. https://doi.org/10.1080/07900627.2012.669520

Fellman, J. B., Hood, E., & Spencer, R. G. M. (2010). Fluorescence spectroscopy opens new windows into dissolved organic matter dynamics in freshwater ecosystems: A review. *Limnology & Oceanography*, *55*(6), 2452–2462. https://doi.org/10.4319/lo.2010.55.6.2452

Frankignoulle, M., Abril, G., Borges, A., Bourge, I., Canon, C., DeLille, B., et al. (1998). Carbon dioxide emission from European estuaries. *Science*, *282*(5388), 434–436. https://doi.org/10.1126/science.282.5388.434

Friedlingstein, P., Jones, M. W., O'Sullivan, M., Andrew, R. M., Hauck, J., Peters, G. P., et al. (2019). Global carbon budget 2019. *Earth System Science Data*, *11*(4), 1783–1838. https://doi.org/10.5194/essd-11-1783-2019

Gao, T., & Wang, H. (2017). Trends in precipitation extremes over the Yellow River basin in North China: Changing properties and causes. *Hydrological Processes*, *31*(13), 2412–2428. https://doi.org/10.1002/hyp.11192

Garnier, J., Vilain, G., Silvestre, M., Billen, G., Jehanno, S., Poirier, D., et al. (2013). Budget of methane emissions from soils, livestock and the river network at the regional scale of the Seine basin (France). *Biogeochemistry*, *116*(1–3), 199–214. https://doi.org/10.1007/s10533-013-9845-1

Gevantman, L. H. (2010). Solubility of selected gases in water. In D. R. Lide (Ed.), *CRC handbook of chemistry and physics* (90th ed., Chapter 8, pp. 80–83). CRC Press.

Hamilton, S. K., & Ostrom, N. E. (2007). Measurement of the stable isotope ratio of dissolved N_2 in ^{15}N tracer experiments. *Limnology and Oceanography: Methods*, *5*(7), 233–240. https://doi.org/10.4319/lom.2007.5.233

He, Y., Wang, X., Chen, H., Yuan, X., Wu, N., Zhang, Y., et al. (2017). Effect of watershed urbanization on N_2O emissions from the Chongqing metropolitan river network, China. *Atmospheric Environment*, *171*, 70–81. https://doi.org/10.1016/j.atmosenv.2017.09.043

Helms, J. R., Stubbins, A., Ritchie, J. D., Minor, E. C., Kieber, D. J., & Mopper, K. (2008). Absorption spectral slopes and slope ratios as indicators of molecular weight, source, and photobleaching of chromophoric dissolved organic matter. *Limnology & Oceanography*, *53*(3), 955–969. https://doi.org/10.4319/lo.2008.53.3.0955

Hu, M., Chen, D., & Dahlgren, R. A. (2016). Modeling nitrous oxide emission from rivers: A global assessment. *Global Change Biology*, *22*(11), 3566–3582. https://doi.org/10.1111/gcb.13351

Hudson, F. (2004). *Sample preparation and calculations for dissolved gas analysis in water samples using a GC headspace equilibration technique, RSKSOP-175* (Revision No. 2, pp. 1–14). U.S. Environmental Protection Agency.

Huguet, A., Vacher, L., Relexans, S., Saubusse, S., Froidefond, J. M., & Parlanti, E. (2009). Properties of fluorescent dissolved organic matter in the Gironde Estuary. *Organic Geochemistry*, *40*(6), 706–719. https://doi.org/10.1016/j.orggeochem.2009.03.002

Jin, H., Yoon, T. K., Begum, M. S., Lee, E.-J., Oh, N.-H., Kang, N., & Park, J.-H. (2018). Longitudinal discontinuities in riverine greenhouse gas dynamics generated by dams and urban wastewater. *Biogeosciences*, *15*(20), 6349–6369. https://doi.org/10.5194/bg-15-6349-2018

Keeling, C. D. (1958). The concentration and isotopic abundances of atmospheric carbon dioxide in rural areas. *Geochimica et Cosmochimica Acta*, *13*(4), 322–334. https://doi.org/10.1016/0016-7037(58)90033-4

Kim, D., Begum, M. S., Choi, J., Jin, H., Chea, E., & Park, J.-H. (2019). Comparing effects of untreated and treated wastewater on riverine greenhouse gas emissions. *APN Science Bulletin*, *9*(1), 88–94. https://doi.org/10.30852/sb.2019.872

Knox, M., Quay, P. D., & Wilbur, D. (1992). Kinetic isotopic fractionation during air-water gas transfer of O_2, N_2, CH_4, and H_2. *Journal of Geophysical Research*, *97*(C12), 20335–20343. https://doi.org/10.1029/92JC00949

Kroeze, C., Dumont, E., & Seitzinger, S. (2010). Future trends in emissions of N_2O from rivers and estuaries. *Journal of Integrative Environmental Sciences*, *7*, 71–78. https://doi.org/10.1080/1943815x.2010.496789

Lauerwald, R., Laruelle, G. G., Hartmann, J., Ciais, P., & Regnier, P. A. G. (2015). Spatial patterns in CO_2 evasion from the global river network. *Global Biogeochemical Cycles*, *29*(5), 534–554. https://doi.org/10.1002/2014GB004941

Lehner, B., Liermann, C. R., Revenga, C., Vörösmarty, C., Fekete, B., Crouzet, P., et al. (2011). High-resolution mapping of the world's reservoirs and dams for sustainable river-flow management. *Frontiers in Ecology and the Environment*, *9*(9), 494–502. https://doi.org/10.1890/100125

Li, S., Lu, X. X., & Bush, R. T. (2013). CO_2 partial pressure and CO_2 emission in the Lower Mekong River. *Journal of Hydrology*, *504*, 40–56. https://doi.org/10.1016/j.jhydrol.2013.09.024

Li, X., Yao, H., Yu, Y., Cao, Y., & Tang, C. (2020). Greenhouse gases in an urban river: Trend, isotopic evidence for underlying processes, and the impact of in-river structures. *Journal of Hydrology*, *591*, 125290. https://doi.org/10.1016/j.jhydrol.2020.125290

Lin, L., Lu, X., Liu, S., Liong, S.-Y., & Fu, K. (2019). Physically controlled CO_2 effluxes from a reservoir surface in the upper Mekong River Basin: A case study in the Gongguoqiao Reservoir. *Biogeosciences*, *16*(10), 2205–2219. https://doi.org/10.5194/bg-16-2205-2019

Maher, D. T., Santos, I. R., Leuven, J. R. F. W., Oakes, J. M., Erler, D. V., Carvalho, M. C., & Eyre, B. D. (2013). Novel use of cavity ring-down spectroscopy to investigate aquatic carbon cycling from microbial to ecosystem scales. *Environmental Science & Technology*, *47*(22), 12938–12945. https://doi.org/10.1021/es4027776

Manaka, T., Ushie, H., Araoka, D., Otani, S., Inamura, A., Suzuki, A., et al. (2015). Spatial and seasonal variation in surface water pCO_2 in the Ganges, Brahmaputra, and Meghna Rivers on the Indian Subcontinent. *Aquatic Geochemistry*, *21*(5), 437–458. https://doi.org/10.1007/s10498-015-9262-2

Marescaux, A., Thieu, V., & Garnier, J. (2018). Carbon dioxide, methane and nitrous oxide emissions from the human-impacted Seine watershed in France. *Science of the Total Environment*, *643*, 247–259. https://doi.org/10.1016/j.scitotenv.2018.06.151

McCallister, S. L., & del Giorgio, P. A. (2008). Direct measurement of the $\delta^{13}C$ signature of carbon respired by bacteria in lakes: Linkages to potential carbon sources, ecosystem baseline metabolism, and CO_2 fluxes. *Limnology & Oceanography*, *53*(4), 1204–1216. https://doi.org/10.4319/lo.2008.53.4.1204

McKnight, D. M., Boyer, E. W., Westerhoff, P. K., Doran, P. T., Kulbe, T., & Andersen, D. T. (2001). Spectrofluorometric characterization of dissolved organic matter for indication of precursor organic material and aromaticity. *Limnology & Oceanography*, *46*(1), 38–48. https://doi.org/10.4319/lo.2001.46.1.0038

Mekonnen, M. M., & Hoekstra, A. Y. (2018). Global anthropogenic phosphorus loads to freshwater and associated grey water footprints and water pollution levels: A high-resolution global study. *Water Resources Research*, *54*(1), 345–358. https://doi.org/10.1002/2017WR020448

Miller, J. B., & Tans, P. P. (2003). Calculating isotopic fractionation from atmospheric measurements at various scales. *Tellus B: Chemical and Physical Meteorology*, *55*(2), 207–214. https://doi.org/10.1034/j.1600-0889.2003.00020.x10.3402/tellusb.v55i2.16697

Milliman, J. D., & Farnsworth, K. L. (2011). *River discharge to the coastal ocean: A global synthesis*. Cambridge University Press. https://doi.org/10.1017/CBO9780511781247

Mook, W. G., Bommerson, J. C., & Staverman, W. H. (1974). Carbon isotope fractionation between dissolved bicarbonate and gaseous carbon dioxide. *Earth and Planetary Science Letters*, *22*(2), 169–176. https://doi.org/10.1016/0012-821X(74)90078-8

MRC: Mekong River Commission. (2019). *State of the basin report 2018, Vientiane, Lao PDR*.

O'Dwyer, M., Butman, D. E., Striegl, R. G., Dornblaser, M. M., Wickland, K. P., Kuhn, C. D., & Bogard, M. J. (2020). Patterns and isotopic composition of greenhouse gases under ice in lakes of interior Alaska. *Environmental Research Letters*. (in press). *15*(10), 105016. https://doi.org/10.1088/1748-9326/abb493

Park, J.-H., Nayna, O. K., Begum, M. S., Chea, E., Hartmann, J., Keil, R. G., et al. (2018). Reviews and syntheses: Anthropogenic perturbations to carbon fluxes in Asian river systems - Concepts, emerging trends, and research challenges. *Biogeosciences*, *15*(9), 3049–3069. https://doi.org/10.5194/bg-15-3049-2018

Parua, P. K. (2010). The Ganga: Water use in the Indian Subcontinent (Vol. 64). Springer Science & Business Media.

Qi, M., Yang, Y., Zhang, X., Zhang, X., Wang, M., Zhang, W., et al. (2020). Pollution reduction and operating cost analysis of municipal wastewater treatment in China and implication for future wastewater management. *Journal of Cleaner Production*, *253*, 120003. https://doi.org/10.1016/j.jclepro.2020.120003

Qin, X., Li, Y. e., Wan, Y., Fan, M., Liao, Y., Li, Y., et al. (2020). Multiple stable isotopic signatures corroborate the predominance of acetoclastic methanogenesis during CH_4 formation in agricultural river networks. *Agriculture, Ecosystems & Environment*, *296*, 106930. https://doi.org/10.1016/j.agee.2020.106930

Qu, B., Aho, K. S., Li, C., Kang, S., Sillanpää, M., Yan, F., & Raymond, P. A. (2017). Greenhouse gases emissions in rivers of the Tibetan Plateau. *Scientific Reports*, *7*(1), 1–8. https://doi.org/10.1038/s41598-017-16552-6

Ran, L., Li, L., Tian, M., Yang, X., Yu, R., Zhao, J., et al. (2017). Riverine CO_2 emissions in the Wuding River catchment on the Loess Plateau: Environmental controls and dam impoundment impact. *Journal of Geophysical Research: Biogeosciences*, *122*(6), 1439–1455. https://doi.org/10.1002/2016jg003713

Ran, L., Lu, X. X., Richey, J. E., Sun, H., Han, J., Yu, R., et al. (2015). Long-term spatial and temporal variation of CO_2 partial pressure in the Yellow River, China. *Biogeosciences*, *12*(4), 921–932. https://doi.org/10.5194/bg-12-921-2015

Rao, G. D., Rao, V. D., & Sarma, V. V. S. S. (2013). Distribution and air-sea exchange of nitrous oxide in the coastal Bay of Bengal during peak discharge period (southwest monsoon). *Marine Chemistry*, *155*, 1–9. https://doi.org/10.1016/j.marchem.2013.04.014

Rao, G. D., & Sarma, V. V. S. S. (2017). Influence of river discharge on the distribution and flux of methane in the coastal Bay of Bengal. *Marine Chemistry*, *197*, 1–10. https://doi.org/10.1016/j.marchem.2017.11.002

Raymond, P. A., Hartmann, J., Lauerwald, R., Sobek, S., McDonald, C., Hoover, M., et al. (2013). Global carbon dioxide emissions from inland waters. *Nature*, *503*(7476), 355–359. https://doi.org/10.1038/nature12760

Raymond, P. A., Zappa, C. J., Butman, D., Bott, T. L., Potter, J., Mulholland, P., et al. (2012). Scaling the gas transfer velocity and hydraulic geometry in streams and small rivers. *Limnology & Oceanography*, *2*(1), 41–53. https://doi.org/10.1215/21573689-1597669

R Development Core Team. (2020). *R: A language and environment for statistical computing*. R Foundation for Statistical Computing. Retrieved from http://www.r-project.org

Regnier, P., Friedlingstein, P., Ciais, P., Mackenzie, F. T., Gruber, N., Janssens, I. A., et al. (2013). Anthropogenic perturbation of the carbon fluxes from land to ocean. *Nature Geoscience*, *6*(8), 597–607. https://doi.org/10.1038/ngeo1830

Richey, J. E., Devol, A. H., Wofsy, S. C., Victoria, R., & Riberio, M. N. G. (1988). Biogenic gases and the oxidation and reduction of carbon in Amazon River and floodplain waters. *Limnology & Oceanography*, *33*(4), 551–561. https://doi.org/10.4319/lo.1988.33.4.0551

Samanta, S., Dalai, T. K., Pattanaik, J. K., Rai, S. K., & Mazumdar, A. (2015). Dissolved inorganic carbon (DIC) and its $\delta^{13}C$ in the Ganga (Hooghly) River estuary, India: Evidence of DIC generation via organic carbon degradation and carbonate dissolution. *Geochimica et Cosmochimica Acta*, *165*, 226–248. https://doi.org/10.1016/j.gca.2015.05.040

Sarma, V. V. S. S., Viswanadham, R., Rao, G. D., Prasad, V. R., Kumar, B. S. K., Naidu, S. A., et al. (2012). Carbon dioxide emissions from Indian monsoonal estuaries. *Geophysical Research Letters*, *39*(3), L03602. https://doi.org/10.1029/2011GL050709

Sato, T., Qadir, M., Yamamoto, S., Endo, T., & Zahoor, A. (2013). Global, regional, and country level need for data on wastewater generation, treatment, and use. *Agricultural Water Management*, *130*, 1–13. https://doi.org/10.1016/j.agwat.2013.08.007

Sawakuchi, H. O., Bastviken, D., Sawakuchi, A. O., Ward, N. D., Borges, C. D., Tsai, S. M., et al. (2016). Oxidative mitigation of aquatic methane emissions in large Amazonian rivers. *Global Change Biology*, *22*(3), 1075–1085. https://doi.org/10.1111/gcb.13169

Sharma, S., Jha, P. K., Ranjan, M. R., Singh, U. K., & Jindal, T. (2017). Water quality monitoring of Yamuna River by using GIS based water quality index in Delhi, India. *International Journal of Current Microbiology and Applied Sciences*, *6*(2), 1249–1263. https://doi.org/10.20546/ijcmas.2017.602.141

Stanley, E. H., Casson, N. J., Christel, S. T., Crawford, J. T., Loken, L. C., & Oliver, S. K. (2016). The ecology of methane in streams and rivers: Patterns, controls, and global significance. *Ecological Monographs*, *86*(2), 146–171. https://doi.org/10.1890/15-1027

Stedmon, C. A., & Bro, R. (2008). Characterizing dissolved organic matter fluorescence with parallel factor analysis: A tutorial. *Limnology and Oceanography: Methods*, *6*(11), 572–579. https://doi.org/10.4319/lom.2008.6.57210.4319/lom.2008.6.572b

Teodoru, C. R., Bastien, J., Bonneville, M.-C., del Giorgio, P. A., Demarty, M., Garneau, M., et al. (2012). The net carbon footprint of a newly created boreal hydroelectric reservoir. *Global Biogeochemical Cycles*, *26*(2), 1–14. https://doi.org/10.1029/2011GB004187

Throckmorton, H. M., Heikoop, J. M., Newman, B. D., Altmann, G. L., Conrad, M. S., Muss, J. D., et al. (2015). Pathways and transformations of dissolved methane and dissolved inorganic carbon in Arctic tundra watersheds: Evidence from analysis of stable isotopes. *Global Biogeochemical Cycles*, *29*, 1893–1910. https://doi.org/10.1016/s0147-6513(02)00089-110.1002/2014gb005044

Tian, M., Yang, X., Ran, L., Su, Y., Li, L., Yu, R., et al. (2019). Impact of Land Cover types on riverine CO_2 outgassing in the Yellow River Source Region. *Water*, *11*(11), 2243. https://doi.org/10.3390/w11112243

Tong, L., Xu, X., Fu, Y., & Li, S. (2014). Wetland changes and their responses to climate change in the "Three-River Headwaters" Region of China since the 1990s. *Energies*, *7*(4), 2515–2534. https://doi.org/10.3390/en7042515

Ulliman, S. L., Korak, J. A., Linden, K. G., & Rosario-Ortiz, F. L. (2020). Methodology for selection of optical parameters as wastewater effluent organic matter surrogates. *Water Research*, *170*, 115321. https://doi.org/10.1016/j.watres.2019.115321

Vannote, R. L., Minshall, G. W., Cummins, K. W., Sedell, J. R., & Cushing, C. E. (1980). The river continuum concept. *Canadian Journal of Fisheries and Aquatic Sciences*, *37*(1), 130–137. https://doi.org/10.1139/f80-017

Wang, H., Yang, Z., Saito, Y., Liu, J. P., & Sun, X. (2006). Interannual and seasonal variation of the Huanghe (Yellow River) water discharge over the past 50 years: Connections to impacts from ENSO events and dams. *Global and Planetary Change*, *50*(3–4), 212–225. https://doi.org/10.1016/j.gloplacha.2006.01.005

Wang, X., He, Y., Yuan, X., Chen, H., Peng, C., Yue, J., et al. (2017). Greenhouse gases concentrations and fluxes from subtropical small reservoirs in relation with watershed urbanization. *Atmospheric Environment*, *154*, 225–235. https://doi.org/10.1016/j.atmosenv.2017.01.047

Weishaar, J. L., Aiken, G. R., Bergamaschi, B. A., Fram, M. S., Fujii, R., & Mopper, K. (2003). Evaluation of specific ultraviolet absorbance as an indicator of the chemical composition and reactivity of dissolved organic carbon. *Environmental Science & Technology*, *37*(20), 4702–4708. https://doi.org/10.1021/es030360x

Weiss, R. F. (1974). Carbon dioxide in water and seawater: The solubility of a non-ideal gas. *Marine Chemistry*, *2*(3), 203–215. https://doi.org/10.1016/0304-4203(74)90015-2

Whitehead, P. G., Sarkar, S., Jin, L., Futter, M. N., Caesar, J., Barbour, E., et al. (2015). Dynamic modeling of the Ganga river system: Impacts of future climate and socio-economic change on flows and nitrogen fluxes in India and Bangladesh. *Environmental Sciences: Processes Impacts*, *17*(6), 1082–1097. https://doi.org/10.1039/c4em00616j

WLE: Water, Land, and Ecosystems—Mekong. (2020). *Mekong hydropower map and portal*. Retrieved from https://wle-mekong.cgiar.org/wp-content/uploads/unnamed-11.jpg

Yang, X., Xue, L., Li, Y., Han, P., Liu, X., Zhang, L., & Cai, W.-J. (2018). Treated wastewater changes the export of dissolved inorganic carbon and its isotopic composition and leads to acidification in coastal oceans. *Environmental Science & Technology*, *52*(10), 5590–5599. https://doi.org/10.1021/acs.est.8b00273

Yoon, T. K., Jin, H., Begum, M. S., Kang, N., & Park, J.-H. (2017). CO_2 outgassing from an urbanized river system fueled by wastewater treatment plant effluents. *Environmental Science & Technology*, *51*(18), 10459–10467. https://doi.org/10.1021/acs.est.7b02344

Yoon, T. K., Jin, H., Oh, N.-H., & Park, J.-H. (2016). Technical note: Assessing gas equilibration systems for continuous pCO_2 measurements in inland waters. *Biogeosciences*, *13*(13), 3915–3930. https://doi.org/10.5194/bg-13-3915-2016

Zhao, M. M., Wang, S.-M., Chen, Y.-P., Wu, J.-H., Xue, L.-G., & Fan, T. T. (2020). Pollution status of the Yellow River tributaries in middle and lower reaches. *Science of the Total Environment*, *722*, 137861. https://doi.org/10.1016/j.scitotenv.2020.137861

Zsolnay, A., Baigar, E., Jimenez, M., Steinweg, B., & Saccomandi, F. (1999). Differentiating with fluorescence spectroscopy the sources of dissolved organic matter in soils subjected to drying. *Chemosphere*, *38*(1), 45–50. https://doi.org/10.1016/S0045-6535(98)00166-0